Intermittent Hypoxia Promotes Functional Neuroprotection from Retinal Ischemia in Untreated First-Generation Offspring: Proteomic Mechanistic Insights

Jarrod C. Harman[1–3] Jessie J. Guidry[2,4] and Jeffrey M. Gidday[1–3,5]

[1]Department of Ophthalmology, School of Medicine, Louisiana State University Health Sciences Center, New Orleans, Louisiana, United States
[2]Department of Biochemistry and Molecular Biology, School of Medicine, Louisiana State University Health Sciences Center, New Orleans, Louisiana, United States
[3]Neuroscience Center of Excellence, School of Medicine, Louisiana State University Health Sciences Center, New Orleans, Louisiana, United States
[4]LSUHSC Proteomics Core Facility, School of Medicine, Louisiana State University Health Sciences Center, New Orleans, Louisiana, United States
[5]Department of Physiology, School of Medicine, Louisiana State University Health Sciences Center, New Orleans, Louisiana, United States

Correspondence: Jeffrey M. Gidday, Department of Ophthalmology, School of Medicine, Louisiana State University, 533 Bolivar Street, CSRB Room 454, New Orleans, LA 70112, USA;
jgidda@lsuhsc.edu.

Received: May 14, 2020
Accepted: August 3, 2020
Published: September 10, 2020

Citation: Harman JC, Guidry JJ, Gidday JM. Intermittent hypoxia promotes functional neuroprotection from retinal ischemia in untreated first-generation offspring: Proteomic mechanistic insights. *Invest Ophthalmol Vis Sci.* 2020;61(11):15. https://doi.org/10.1167/iovs.61.11.15

Purpose. Stress can lead to short- or long-term changes in phenotype. Accumulating evidence also supports the transmission of maladaptive phenotypes, induced by adverse stressors, through the germline to manifest in subsequent generations, providing a novel mechanistic basis for the heritability of disease. In the present study in mice, we tested the hypothesis that repeated presentations of a nonharmful conditioning stress, demonstrated previously to protect against retinal ischemia, will also provide ischemic protection in the retinae of their untreated, first-generation (F1) adult offspring.

Methods. Swiss–Webster ND4 outbred mice were mated following a 16-week period of brief, every-other-day conditioning exposures to mild systemic hypoxia (repetitive hypoxic conditioning, RHC). Retinae of their 5-month-old F1 progeny were subjected to unilateral ischemia. Scotopic electroretinography quantified postischemic outcomes. The injury-resilient retinal proteome was revealed by quantitative mass spectrometry, and bioinformatic analyses identified the biochemical pathways and networks in which these differentially expressed proteins operate.

Results. Significant resilience to injury in both sexes was documented in F1 mice derived from RHC-treated parents, relative to matched F1 adult progeny derived from normoxic control parents. Ischemia-induced increases and decreases in the expression of many visual transduction proteins that are integral to photoreceptor function were abrogated by parental RHC, providing a molecular basis for the observed functional protection.

Conclusions. Our proteomic analyses provided mechanistic insights into the molecular manifestation of the inherited, injury-resilient phenotype. To our knowledge, this is the first study in a mammalian model documenting the reprogramming of heritability to promote disease resilience in the next generation.

Keywords: retina, ischemia, neuroprotection, epigenetics, proteomics, bioinformatics, intergenerational, preconditioning, resilience

Epigenetics drive cellular responses to stress and environmental change in the form of changes in gene expression,[1] which in some instances exert long-lasting effects. As examples, early life stress can impact a variety of neuropsychiatric conditions later in life.[2,3] Similarly, cardiovascular disease, cancer, and even aging itself are influenced by a myriad of adverse stress stimuli experienced during childhood.[4,5] In fact, epigenetic modifications secondary to stress and environmental change not only can affect phenotypes across the lifespan but can also affect phenotypes in progeny. Accumulating evidence documents the intergenerational and transgenerational passage of phenotypes in a number of species,[6–8] including mammals.[9–11] That this also occurs in humans, beyond imprinting, is strongly suggested by a broad set of elegantly curated epidemiological data.[12,13] The vast majority of research in these aforementioned fields of study has focused on identifying pathological phenotypes and disease susceptibility

resulting from previously presented adverse stressors. Rare is the finding that adaptive phenotypes can be induced by nonharmful stressors, despite the likelihood that such beneficial responses actually represent the largely unrecognized other half of the lifespan/inheritance fields.

Several decades of preclinical studies in cardiac[14] and cerebral[15] conditioning medicine consistently confirm that epigenetically mediated changes in gene expression, induced in response to a nonharmful conditioning stimulus, promote a transient resilience to acute tissue ischemia. From these and related studies, it is becoming increasingly clear that the magnitude, duration, and frequency of the conditioning stimulus dictate not only whether the induced phenotypic response is adaptive or maladaptive but also that the frequency, or intermittent nature, of the stimulus proportionally affects the duration of said response.[16–20] Such findings raise the possibility of leveraging repetitive conditioning stimuli to induce, throughout the lifespan, beneficial modifications in gene expression that promote health and disease resiliency. In turn, repetitive conditioning may even induce adaptive epigenetic changes in the germline that promote injury resilience in offspring.

To test the hypothesis that this type of cytoprotective intergenerational inheritance occurs in the central nervous system of mammals, we used a well-established mouse model of transient, unilateral retinal ischemia. The worldwide incidence of ischemic retinopathies, including nonproliferative diabetic retinopathy, glaucoma, age-related macular degeneration, and acute ischemia secondary to branch and central retinal artery occlusion, is significant[21–24]; however, efficacious therapies designed to protect the retina against their consequent blindness and related visual morbidities have yet to be developed. To ensure rigor, we quantified postischemic retinal function by electroretinography in large cohorts. Repetitive hypoxic conditioning (RHC), which has a human correlate in remote limb conditioning,[25] served as the conditioning stimulus. We also investigated the mechanistic underpinnings of the intergenerational neuroprotected phenotype by performing quantitative mass spectrometry (MS) on retinae of F1 mice derived from RHC-treated parents and untreated control parents. Subsequent bioinformatic analyses of these novel protein expression profiles identified photoreceptor cell-specific and more ubiquitous cellular signaling pathways and networks that likely underlie this inherited resilience to ischemic injury.

Materials and Methods

All procedures were approved by our Institutional Animal Care and Use Committee and adhered to ARRIVE guidelines, the National Institutes of Health Guide for the Care and Use of Laboratory Animals, and the ARVO Statement for the Use of Animals in Ophthalmic and Vision Research.

Repetitive Hypoxic Conditioning

Outbred SWND4 mice of both sexes were obtained from Envigo (Indianapolis, IN, USA) at 7 to 8 weeks of age, group-housed by sex (five males per cage and five females per cage), and maintained on a 12-hour light/dark cycle with mouse chow provided ad libitum. After a 2-week period of acclimation to our animal facility, our RHC treatment was initiated. The mice remained in their home cages during the hypoxia exposures. Following removal of the lid covers, the cages were placed through an air-tight, sealable door into a large, gas-tight chamber (BioSpherix, Ltd., Parish, NY, USA); up to 10 cages could fit into the chamber simultaneously. Thereafter, the ambient oxygen tension in the chamber was reduced to, and maintained at, 11% by flushing 100% nitrogen gas through the chamber (vent ports located opposite to inlet source) in a feedback-regulated manner, controlled by an oxygen sensor with light-emitting diode readout. A two-point (electronic zero, 21%) calibration of the oxygen sensor was performed weekly. The oxygen tension was confirmed at regular intervals using a portable oxygen sensor (VTI Oxygen Analyzer; Vascular Technology, Nashua, NH, USA) placed within the chamber. The oxygen tension in the chamber fell from 21% to 11% in ~5 minutes; thereafter, the mice remained in the chamber for 1 or 2 hours (see treatment protocol below). At the end of the exposure period, the door to the chamber was opened, and the cages were sequentially moved into the ambient air of the housing room; the lids were replaced and the cages were returned to the cage rack.

The RHC protocol we followed involved exposing the mice to 11% oxygen three times per week (Monday, Wednesday, and Friday) for 16 consecutive weeks. During the initial 8 weeks, the duration of exposure was 1 hour; the duration of exposure was increased to 2 hours during the final 8 weeks to prevent potential habituation to the stimulus. Exposures were conducted between 8 AM and 12 PM. Age- and sex-matched mice served as normoxic controls and were run in parallel; that is, when cages of experimental mice were moved to and from the chamber for RHC exposure, the cages of control mice were also moved to and from an open shelf in the same housing room, and their cage lids were removed to expose them to the normoxic room air for an equivalent period of time (1 or 2 hours).

At the gross examination level, we observed no adverse effects of the RHC stress on our F0 animals. During the initial couple of exposures to hypoxia, the mice tended to huddle together and remain relatively immobile for the duration of treatment, but by the third week of treatment they exhibited normal cage behaviors during the hypoxic exposure. Increasing the duration of RHC to 2 hours starting the ninth week of treatment produced no further behavioral changes of note. Although the F0 animals continued to gain weight, as expected, during the 16-week period of treatment there were no significant changes in body weight between the normoxic control mice and the RHC-treated mice at any time point (data not shown). In additional cohorts, we also found no quantitative differences in hippocampal CA1 pyramidal cell density between F0 parental groups, as reported previously.[26] Fecundity was also unaffected by the 16-week RHC treatment; the F0 normoxic control breeders gave birth to as many litters as the F0 RHC-treated breeder pairs, and neither litter size nor male/female distributions varied between groups. In random, intermittent inspections prior to weaning at 21 days of age, we did not observe any differences in maternal/paternal care behaviors of the RHC-treated F0 parents and the untreated control F0 parents.

The eyes and outward appearance of F1 progeny from RHC-treated F0 mice also appeared completely normal upon gross examination at all ages, from pups through 5 months of age. Retinal morphology was assessed in additional cohorts of 5-month-old F1 mice derived from RHC-treated F0 parents and untreated control F0 parents using spectral-domain optical coherence tomography (SD-OCT; Heidelberg Engineering, Heidelberg, Germany). Briefly, scans were obtained of an 8.8-mm^2 circular area in the supe-

rior retina bordering the optic disc. Total retinal thickness and the thickness of individual layers (nerve fiber, ganglion cell, inner plexiform, inner nuclear, outer plexiform, outer nuclear, and photoreceptor) were quantified following segmentation by Heidelberg software. Results were analyzed, by sex, using 2-way ANOVA.

Retinal Ischemia and Functional Outcomes—Experimental Design

Mice received from the vendor, designated the F0 generation, were randomized to RHC or normoxic control groups, with equal numbers of males and females receiving the RHC treatment. Overall, two cohorts of F0 mice were studied; that is, two cohorts of F0 mice derived from two separate shipments from the vendor were exposed to 16 weeks of RHC (or normoxia) and subsequently bred to generate two cohorts of F1 generation mice. In sum, five breeding pairs of RHC-treated F0 mice and four breeding pairs of untreated F0 mice were used to generate 10 litters each of F1 mice that were used for functional outcome analyses in this study.

Breeding pairs of mice were established 4 days after the last hypoxia exposure by placing a single male with a single female in a clean cage. Experimental breeder groups, in which both male and female F0 mice received RHC, and control breeder groups, in which both male and female F0 mice were normoxic controls, were established. Their respective F1 progeny we termed F1-*RHC mice (the asterisk denotes that these F1 mice were never exposed directly to our RHC stimulus), and F1-control mice. Ten F1 litters were included in the analysis, with the time between the last hypoxia exposure and conception of the given litter recorded. F1 mice were housed by sex in groups with a minimum of two and maximum of five mice per cage. When F1 mice reached at least 4 months of age, they were subjected to 30-minute unilateral retinal ischemia (see below). Electroretinography was used to quantify the extent of ischemic injury 1 week following ischemia (see below).

Retinal Ischemia

Three or 4 days after baseline electroretinography (see below), F1 mice were anesthetized with ketamine/xylazine (100 mg/kg ketamine/10 mg/kg xylazine) intraperitoneally, and the right eye (RE) was subjected to 30 minutes of unilateral, normothermic retinal ischemia; the left eye (LE) was used as an internal control. Mice were thermoregulated at a body temperature of 37° ±0.5°C throughout the procedure using a temp-set YSI 402 Micro Temperature Controller (Yellow Springs Instruments, Yellow Springs, OH, USA) system with a rectal probe reference. Corneas were hydrated using an ophthalmic balanced salt solution. To induce retinal ischemia, a micromanipulator-mounted, 32-gauge needle (attached to a 0.9% normal saline reservoir) was inserted laterally into the anterior chamber to avoid puncturing the lens. The reservoir was then elevated (178 cm) to increase intraocular pressure above systolic blood pressure, with the resultant ischemia confirmed visually in every animal by observing retinal blanching with a dissecting microscope. After 30 minutes, the needle was slowly withdrawn, and bacitracin-zinc/neomycin ophthalmic antibiotics were applied to both eyes. Mice were monitored in a warm holding cage during their acute recovery following the procedure and then returned to our vivarium for 1 week, at which point we performed postischemic electroretinography (ERG) to functionally assess outcome.

Electroretinography

To account for small, but potentially significant diurnal, hormonal, or biological variances in retinal functional activity, pre- and postischemic ERGs were recorded at approximately the same time of day for any given animal. Mice were dark adapted overnight prior to the performance of (scotopic) ERGs. All procedures conducted in the ERG laboratory were performed in complete darkness by the same technician using only a dim red headlamp (Princeton Tec Fred headlight, 625 ± 5 nm; Princeton Tec, Trenton, NJ, USA). Mice were anesthetized using intraperitoneal ketamine/xylazine (100 mg/kg ketamine/10 mg/kg xylazine) and placed on a thermoregulating table that maintained body temperature at 37° ± 0.5°C throughout the ERG recording. Bilateral ERGs, obtained using gold electrodes and a ColorDome binocular flash stimulator (Diagnosys LLC, Lowell, MA, USA) system, were used to quantify the ability of the retina to respond to a series of light flashes of increasing intensity. Responses were measured using an eight-step protocol that exposed mice to a series of flashes with intensities ranging from 0.00025 cd·s/m^2 6500K white light (step 1) to 5000 cd·s/m^2 xenon (step 8). Peak amplitudes were those recorded at step 7 (250 cd·s/m^2 xenon), with step 8 (not shown in figures) being used only to confirm that peak response amplitudes were achieved at step 7. Three or 4 days after baseline ERG, mice were subjected to the unilateral retinal ischemia described in detail above; thereafter, mice were returned to our vivarium, and on postischemic day 7 scotopic ERGs were acquired, again following the same eight-step, increasing flash intensity protocol as just described for baseline recordings.

ERG waveforms were analyzed visually and in raw quantitative format exported into Excel (Microsoft Corp., Redmond, WA, USA). Exclusion criteria included the following: greater than 25% deviation between the RE and left eye LE in a-wave or b-wave amplitude at baseline, surgical complications, or animals becoming "light" under anesthesia and requiring additional anesthesia. Any mouse that, for any reason, did not survive through the postischemic ERG time point was not included in any dataset.

ERG waveform data from the ischemic eye were normalized to those in the contralateral eye of each individual mouse as follows: The RE/LE ratios were determined for baseline and postischemic measurements at all steps of the protocol, and the postischemic RE/LE ratio was then divided by the baseline RE/LE ratio to determine, as a percentage, the overall loss of amplitude resulting from preceding ischemia.

ERG data were statistically analyzed using Stata SE15 (StataCorp, College Station, TX, USA). Unpaired *t*-tests followed by Mann–Whitney comparison ranking were performed in Prism 8.3.0 (GraphPad, San Diego, CA, USA) to compare individual step and peak electroretinogram amplitudes. Two-way ANOVA analysis was performed to compare individual ERG steps by treatment and sex, followed by Šidák multiple comparisons testing.

Mass Spectrometry and Proteomic Analyses

Experimental Design Platform. To probe the mechanistic basis of this intergenerational adaptive phenotype that we documented at the functional level by electroretinography, we performed quantitative, discovery-based proteomic analyses of retinae collected from F1 animals born to RHC-treated parents (F1-*RHC mice) and

Investigative Ophthalmology & Visual Science

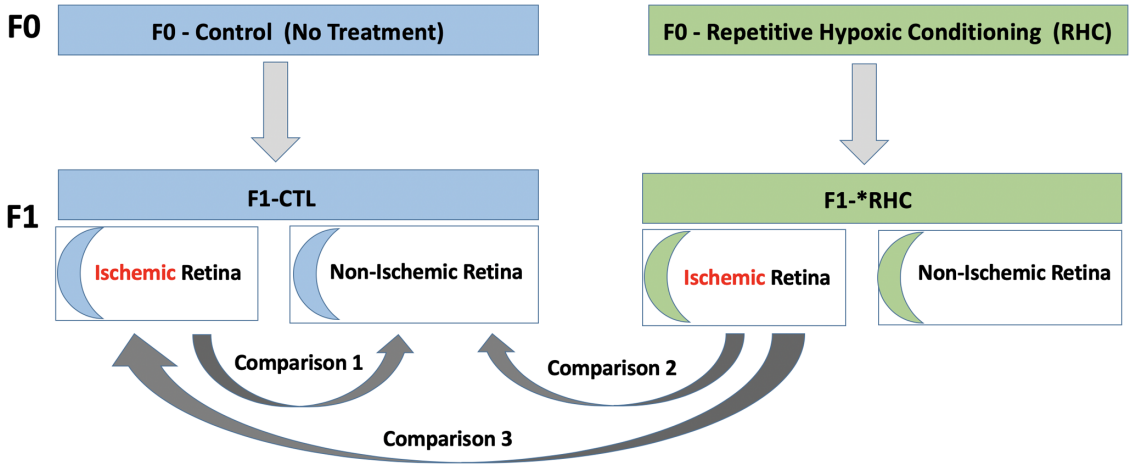

Figure 1. Three differential retinal proteomes compared by mass spectrometry. Shown are the differential proteomes resulting from F0 RHC and F1 ischemia, as variables, expressed as relative differences (ratios) or comparisons in the text. As such, they serve as a reference platform for describing experimental outcomes.

from F1 animals born to normoxic control parents (F1-control mice, F1-CTL), selecting animals that were most representative of the mean loss of ERG waveform magnitude. Specifically, ischemic and nonischemic retinae from four age-matched males (22 ± 2 weeks old; two animals derived from control parents and two animals derived from RHC-treated parents) were collected 10 days after ischemia (3 days after postischemic ERG). This established three experimental groups for which we identified and analyzed the respective differential proteomes:

Comparison 1 (C1)—Ischemic retinae of F1 mice derived from untreated control F0 parents versus nonischemic retinae of F1 mice derived from untreated control F0 parents

Comparison 2 (C2)—Ischemic retinae of F1 mice derived from hypoxic F0 parents versus nonischemic retinae of F1 mice derived from untreated control F0 parents

Comparison 3 (C3)—Ischemic retinae of F1 mice derived from hypoxic F0 parents versus ischemic retinae of F1 mice derived from untreated control parents

These comparisons are illustrated in Figure 1. We also collected and performed mass spectrometry on the nonischemic retinae from F1 mice to understand how parental RHC affected the baseline retinal proteome prior to ischemia, an important priming step that contributes to the overall ischemic resilience. However, given our focus here on postischemic proteomes and journal space limitations, findings from this experimental group are beyond the scope of the present investigation and will be published separately.

Sample Collection and Preparation. Following a single incision across the sclera with a no. 10 blade scalpel, the retina and lens were removed and subsequently separated from one another using sterile forceps. Retinal tissues harvested in this manner did not include Bruch's membrane, choriocapillaris, or eyecup/retinal pigment epithelium.

Discovery-Based Proteomics Using Tandem Mass Tags and Liquid Chromatography–Mass Spectrometry. Samples were prepared for discovery-based quantitative proteomic analysis by the addition of 1% SDS and sonication until completely homogeneous. The protein concentration was determined using a BCA Protein Assay Kit (Thermo Fisher Scientific, Waltham, MA, USA). Based on the protein concentration, 100 µg of each sample was prepared for trypsin digestion by reducing the cysteines with *tris*(2-carboxyethyl)phosphine followed by alkylation with iodoacetamide. After chloroform–methanol precipitation, each protein pellet was digested with trypsin overnight at 37°C. The digested product was labeled using a TMT10-Plex Isobaric Label Reagent Set (Thermo Fisher Scientific) according to the manufacturer's protocol and stored at –80°C until further use.

An equal amount of each tandem mass tag (TMT)-labeled sample was pooled together in a single tube and Sep-Pak purified (Waters Chromatography Ireland, Ltd., Dublin, Ireland) using acidic reversed-phase conditions. After drying to completion, an offline fractionation step was employed to reduce the complexity of the sample. The sample was brought up in 10-mM ammonium hydroxide, pH 10. This mixture was subjected to basic pH reversed-phase chromatography (Dionex UltiMate 3000; Thermo Fisher Scientific). Briefly, the fractions were ultraviolet (UV) monitored at 215 nm for an injection of 100 µL at 0.1 mL/min with a gradient developed from 10-mM ammonium hydroxide (pH = 10) to 100% acetonitrile (ACN) over 90 minutes. A total of 48 fractions (200 µL each) were collected in a 96-well microplate and recombined in a checkerboard fashion to create 12 "super fractions" (original fractions 1, 13, 25, and 37 became new super fraction 1, etc.; original fractions 2, 14, 26, and 38 became new super fraction 2, etc.).[27] The 12 super fractions were then run on a Dionex UltiMate 3000 nano-flow system coupled to a Thermo Fisher Scientific Fusion Orbitrap mass spectrometer. Each fraction was subjected to a 90-minute chromatographic method employing a gradient from 2% to 25% ACN in 0.1% formic acid (ACN/FA) over the course of 65 minutes, a gradient to 50% ACN/FA for an additional 10 minutes, a step to 90% ACN/FA for 5 minutes, and a 10-minute re-equilibration into 2% ACN/FA. Chromatography was carried out in a "trap-and-load" format using a PicoChip source (New Objective, Inc., Woburn, MA, USA) and PepMap 100 C18 LC Columns (5 µm, 100 A). The separation column was PicoChip ReproSil-Pur C18-AQ (3 µm, 120 A, 105 mm). The entire run was at a flow rate of 0.3 µL/min. Electrospray was achieved at 2.6 kV.

TMT data acquisition utilized an MS3 approach for data collection, as previously described.[28] Survey scans (MS1) were performed in the Orbitrap utilizing a resolution of 120,000. Data-dependent MS2 scans were performed in the linear ion trap using a collision-induced dissociation of 25%. Reporter ions were fragmented using high-energy collision dissociation (HCD) of 65% and detected in the Orbitrap using a resolution of 50,000. This was repeated for a total of three technical replicates. The three runs of 12 super fractions were merged and searched using the Sequest HT node of Proteome Discoverer 2.2 (Thermo Fisher Scientific). The Protein FASTA database was *Mus musculus*, FASTA ID = SwissProt, tax ID = 10090, version 2017-10-25. Static modifications included TMT reagents on lysine and N-terminus (+229.163); carbamidomethyl on cysteines (+57.021); dynamic phosphorylation of serine, threonine, and tyrosine (+79.966 Da); and dynamic modification of oxidation of methionine (+15.9949). Parent ion tolerance was 10 ppm, fragment mass tolerance was 0.6 Da, and the maximum number of missed cleavages was set to 2. Only high-scoring peptides were considered utilizing a false discovery rate of <1%, and only one unique high-scoring peptide was required for inclusion of a given identified protein in our results. Our mass spectrometry proteomics data have been deposited to the ProteomeXchange Consortium via the PRIDE partner repository[29] with the dataset identifier PXD014769.

Validation of Discovery-Based Proteomics Using Parallel Reaction Monitoring. We used parallel reaction monitoring (PRM) methodology, a targeted proteomic workflow approach, to validate the quantification of selected proteins of interest. Although discovery-based TMT quantitative proteomics can provide relative abundances across all samples in the analysis set, it suffers in absolute quantitation because it can represent a single snapshot in time. During PRM, only peptides with unique sequences for the targeted proteins are considered, and area under the curve gives much better quantitative resolution.[30] We chose to validate by PRM methodology heat shock protein B, secretoglobin 2B20, and β-crystallin A1; these (and other) proteins could not be validated using Western blotting because of the lack of commercially available antibodies. Peptides were selected for each protein of interest that met the following criteria: no missed trypsin cleavages, no cysteines, no methionines, having between 7 and 15 amino acids, and being unique in that the peptide sequence could differentiate between other isoforms for the said protein of interest. Only peptides with a minimum of six transitions were selected for inclusion. After testing for best flyers, ^{13}C-labeled Absolute Quantitation (AQUA) peptides (Thermo Fisher Scientific) were synthesized to use as internal reference standards, with either a^{13}C-labeled C-terminal heavy arginine or lysine residue. These AQUA peptides are identical in sequence to endogenous peptide sequences (provided below) and have the same liquid chromatography retention time; however, they contain heavy isotopic carbon and nitrogen atoms to be differentiated during mass spectrometry, thus allowing fold differences to be compared directly to known spiked amounts of AQUA peptide.

Heat Shock Protein B LFDQAFGVPR
Secretoglobin 2B20 SILDYISK
β-Crystallin A1 WDAWSGSNAYHIER

Based on the protein concentration, 50 µg of each sample was prepared for trypsin digestion by reducing the cysteines with dithiothreitol followed by alkylation with iodoacetamide. After chloroform–methanol precipitation, each protein pellet was digested with trypsin overnight at 37°C. Five micrograms of each tryptic digestion of all unknown mouse retina samples were spiked with 3.5 pmol of each heavy peptide, and sample acquisition was randomized to account for any instrument drift over time. The chromatography and MS setups were as described previously. Chromatographic runs 68 minutes long were employed, with gradient conditions as described above. Data-independent acquisition was employed for the selected peptide sequences, and transitions were recorded with the following settings: isolation m/z window of 1.4, Orbitrap resolution of 60,000, automatic gain control target value of 5×10^5, injection time of 100 ms, HCD collision of 30, and m/z scan range of 100 to 1500.

Acquired PRM data were processed using Skyline software.[31] Peak integration was performed automatically and then reviewed individually for accuracy. Manual curation was based on spectra meeting the following criteria for acceptance: consistencies in retention time and transition retention time and all matching spectra having a dot product of at least 0.8 congruency with library spectra. Quantities were expressed as a ratio to known heavy peptide concentrations, converted to fmols/5µg total protein, and exported into CSV files for graphing using BioVinci 1.1.5 data visualization software (BioTuring, Inc., San Diego, CA, USA).

Bioinformatic Analyses

Core Analyses. Following completion of data acquisition and analysis in Proteome Discoverer 2.2, subsequent bioinformatic analyses were performed using Panther GeneGo, STRING, and Qiagen Ingenuity Pathway Analysis (IPA) software (Qiagen, Hilden, Germany). Multiple bioinformatic platforms were used to cross-reference proteins and resolve inconsistencies that could arise due to variable protein IDs across different libraries, incorrect classifications, or scheduled update differences between software packages. One initial core analysis was performed in IPA for each individual comparison (see Results for details) using all of the high-confidence data within the dataset. Subsequent analyses were performed to refine the data using strict and mild filters, allowing for insights into highly conserved pathways, as well as potential mechanistic pathways.

When annotating and applying filters for the dataset uploaded to IPA, the following criteria were considered and/or applied: Only Sequest HT scoring peptides were analyzed. Those meeting a significance threshold with a minimum abundance ratio of $\geq$1.5 fold change (FC) up or down, as well as statistically significant P values ($P < 0.05$), were considered in the strict analysis. Proteins meeting a significance threshold with a minimum abundance ratio of $\geq$1.2 FC and those with $P \leq 0.5$ were considered in the mild analysis. Both the strict and mild datasets were reviewed to observe any overlap of top-scoring canonical pathways, upstream regulators, and biological functions. The strict filter was applied to identify the top five hits in the above-mentioned categories for each comparison; the mild filter was applied to procure the bioinformatics schematics shown

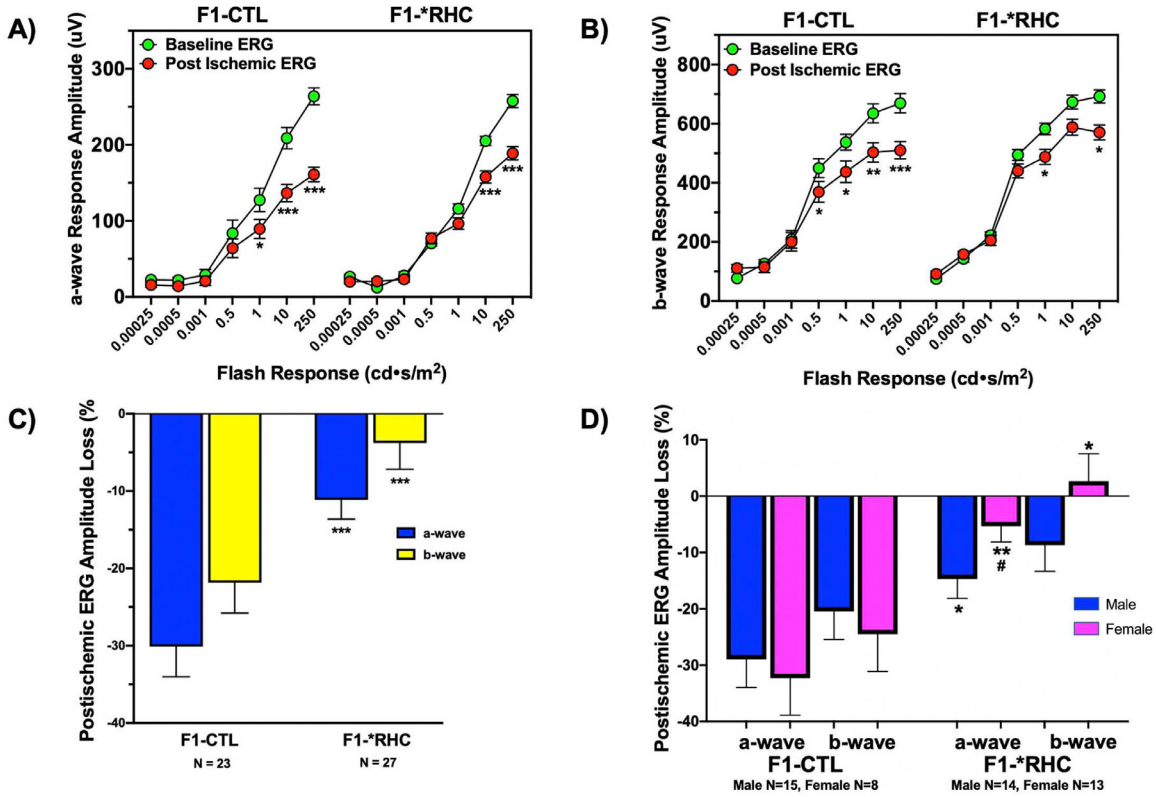

Figure 2. Inherited neuroprotection demonstrated functionally by scotopic ERG. ERG a-wave **(A)** and b-wave **(B)** amplitudes (in microvolts) as a function of increasing light intensity, at pre-ischemic baseline (*green*) and at 7 days postischemia (*red*) for naïve F1 mice derived from untreated F0 parents (F1-CTL) and naïve F1 mice derived from F0 parents treated with RHC prior to mating (F1-*RHC). **(C)** Data from the same F1-control (F1-CTL; $n = 23$) and F1-hypoxia (F1-*RHC; $n = 27$) groups, shown as normalized reductions in a-wave and b-wave amplitudes in the ischemic eye relative to the nonischemic eye at the highest light intensity (250 cd·s/m^2). **(D)** Normalized reductions in a-wave and b-wave amplitudes in the ischemic eye relative to the nonischemic eye at the highest light intensity, by sex (F1-CTL, $n = 15$ males and 8 females; F1-*RHC, $n = 14$ males and 13 females). Mean ± SEM. $^{*}P < 0.05$–0.005, $^{**}P < 0.004$–0.0005, $^{***}P < 0.0002$–0.00005 versus respective baseline ERG waveform amplitude (**A** and **B**), or respective waveform in the F1-CTL group (**C** and **D**); $^{\#}P \leq 0.05$ versus corresponding waveform in male mice (**D**).

in this manuscript. These strict/mild criteria were subjectively defined for every dataset in order to have enough protein and gene IDs to produce meaningful results, which is difficult if the filters applied are too strict, and there is a risk of too many false positives if the applied filters are too mild. Each of the three comparisons was additionally analyzed collectively in IPA using a comparison analysis that equated specific bioinformatic output variables across these three experimental conditions. In all of our bioinformatics analyses, a z-score threshold $> \pm 2$ was applied, which represents a $P < 0.05$ metric for the non-randomness of directionality of a given dataset. For more detailed information on how Qiagen IPA handles these issues in its bioinformatic analyses platform, see http://qiagen.force.com/KnowledgeBase/KnowledgeIPAPage?id = kA41i000000L5ofCAC.

The bioinformatics reported herein are descriptive of the entire proteomic TMT-multiplex experiment, (2) F1-CTL × (2) F1-*RHC, described above, including the core analysis summary report and additional comparison analyses of the top canonical pathways, top molecular and cellular functions, and top upstream regulators. IPA analysis content information includes the following: report date: 2019-11-22; report ID: 18557437; content version: 49309495 (release date: 2019-08-30).

Results

Parental Hypoxia Provides Functional Protection Against Retinal Ischemia in Adult Offspring

To assess whether epigenetics-mediated resilience to retinal ischemic injury induced by RHC in the parental generation[16] is a phenotype that can be inherited by their first-generation offspring, we used scotopic ERG to measure postischemic retinal function in adult, first-generation (F1) progeny born to RHC-treated parents, and in matched F1 progeny born to matched (untreated) control parents. As shown in Figure 2, retinal ischemia in F1 control mice (F1-CTL, derived from normoxic control parents) resulted in a 39% and 27% reduction in a-wave (Fig. 2A) and b-wave (Fig. 2B) amplitudes at the highest flash intensity, respectively, relative to their pre-ischemic baseline responses. In contrast, the extent of a-wave and b-wave amplitude loss was reduced by only 20% and 17%, respectively, in the ischemic retinae of F1 mice born to RHC-treated parents (F1-*RHC). As shown in Figure 2C, when ERG waveform amplitudes of the ischemic retinae were normalized within each animal to their respective contralateral nonischemic retinae for both groups, retinae of mice derived from F1 controls ($n = 23$)

exhibited losses of 30% ± 4% and 22% ± 4% in a-wave and b-wave amplitudes as a result of ischemia, whereas mice derived from RHC-treated parents showed losses of only 11% ± 2% ($P < 0.0001$) and 4% ± 3% ($P < 0.0005$), respectively, in a-wave and b-wave amplitudes. That this protective effect resulted from true ischemic resiliency and not any treatment-induced shift in baseline reactivity is borne out by our documentation in the very same animals that no differences in the baseline, pre-ischemic a-wave and b-wave amplitudes existed between the F1-CTL and F1-*RHC groups in response to any flash intensity (Supplementary Figs. S1a–S1h). When analyzed by sex, we found that F1-CTL male mice had significantly higher ERG responses at baseline for ERG steps 4 to 7 (Supplementary Figs. S1i–S1k) and that male mice exhibited a greater loss of function at 10 days postischemia relative to their female counterparts (Fig. 2D).

Parental Hypoxia Does Not Affect Retinal Morphology in Adult Offspring

Despite having no effect on baseline ERG responses in adult offspring, as well as protecting against ischemia, we also sought to document that our parental RHC treatment did not affect retinal morphology in their adult offspring. SD-OCT imaging of total retinal thickness, as well as the thickness of seven individual retinal layers, in F1 mice derived from untreated and RHC-treated parents did not reveal significant differences in any thickness metric as a result of treatment, even when broken down by sex (Fig. 3). Similarly, no significant differences were found between the two groups of F1 mice with respect to the volume of any of these layers nor total retinal volume (data not shown). These results support the notion that exposing adult mice to the intensity, duration, and frequency of systemic hypoxia that we used, as well as the overall duration of treatment that defined our RHC stimulus, causes no identifiable changes in the retinal morphology of their adult F1 offspring, consistent with the aforementioned lack of functional differences at the level of baseline scotopic ERGs.

Mass Spectrometry Validation

Our proteomic dataset was validated using AQUA peptides in conjunction with PRM, described in detail in Materials and Methods. We elected to perform PRM in lieu of immunoblotting as many of our proteins of interest are isoforms that we were unable to selectively target with an antibody-based Western blot approach. Moreover, the three differentially expressed proteins chosen for PRM had $P > 0.05$, indicating that the expression changes for these proteins required validation. Figure 4 shows the absolute PRM results alongside the relative TMT results for three aforementioned proteins of interest (heat shock protein B, secretoglobin 2B20, and β-crystallin A1). Note that the TMT quantitation (relative) and PRM quantitation (absolute) trend in the same manner, cross-validating results across sample datasets.

Proteomic/Bioinformatic Analyses

Overall, 4175 retinal proteins were identified in our dataset, 4041 with quantitation, which were subsequently uploaded into IPA for bioinformatic analyses of a net 1432 analysis-ready proteins, after applying mild filtering as described in Materials and Methods. The Table provides the top 10 upregulated and top 10 downregulated proteins, based on abundance/fold change, for each of the three experimental group comparisons of interest (Fig. 1) that we will use herein to reference all data displays. Supplementary Table S1 provides an expanded list that includes the top 100 differentially expressed proteins for each comparison. Volcano plots generated for each comparison (Fig. 5) provide a global quantitative picture of protein distributions, based on both fold change and statistical significance, for each of the 4041 proteins identified. Companion heat maps (Fig. 5) highlight the distinct expression profiles for the top 500 differentially expressed proteins in each comparison.

The Postischemic Response—Comparison 1

Comparing the proteome of ischemic retinae in control F1 mice derived from untreated parents to the proteome of nonischemic retinae in control F1 mice derived from untreated parents (Fig. 1)—what we term herein as the control ischemic response, or Comparison 1 (C1) (Table and Supplementary Table S1)—identified the differentially expressed proteins that defined the phenotype of this tissue 10 days postischemia. This included 411 proteins expressed in higher abundance and 80 proteins expressed in lower abundance (491 differentially expressed proteins in total). We found that 233 of the 411 differentially upregulated proteins and 38 of the 80 differentially downregulated proteins were not differentially expressed in response to ischemia in mice derived from RHC-treated parents.

Bioinformatic analyses of the dataset characterizing the control ischemic response yielded the following (IPA-defined) top five enriched canonical pathways (including the number of differentially expressed proteins out of the total number of proteins in the pathway, along with the P value of overlap) that are enriched in proteins that were differentially expressed in response to ischemia: (1) acute phase response signaling (26/179 proteins, $P = 5.5E-21$); (2) LXR/RXR activation (17/121 proteins, $P = 7.0E-14$); (3) FXR/RXR activation (17/126 proteins, $P = 1.4E-13$); (4) coagulation system (9/35 proteins, $P = 2.0E-10$); and (5) RhoGDI signaling (14/180 proteins, $P = 3.1E-8$).

The top five downstream molecular and cellular functions (including the number of proteins in the pathway and the P value range) defining the control ischemic response were (1) cellular movement (117 proteins, $P = 5.3E-6–4.0E-23$); (2) cellular assembly and organization (111 proteins, $P = 4.2E-6–1.7E-18$); (3) protein synthesis (68 proteins, $P = 4.1E-6–2.4E-17$); (4) cell-to-cell signaling and interaction (97 proteins, $P = 5.0E-6–1.5E-16$); and (5) cellular compromise (47 proteins, $P = 3.6E-06–1.6E-16$). The top five upstream regulators (with P values) of the control ischemic response (the upstream molecules responsible for the regulation patterns observed for this particular response) were (1) multifunctional regulator TGF-β1 ($P = 2.3E-18$); (2) prolactin (PRL, $P = 1.5E-16$); (3) tumor suppressor p53 (TP53, $P = 4.8E-15$); (4) IL-6 ($P = 1.7E-12$); and (5) chromatin-regulating high mobility group nucleosome-binding domain containing protein 3 (Hmgn3, $P = 2.2E-12$).

Parental Hypoxia Modifies the Postischemic Response—Comparison 2

The retinal proteomic response to ischemia in F1 mice born to RHC-treated F0 parents (F1-*RHC), relative to the

Investigative Ophthalmology & Visual Science

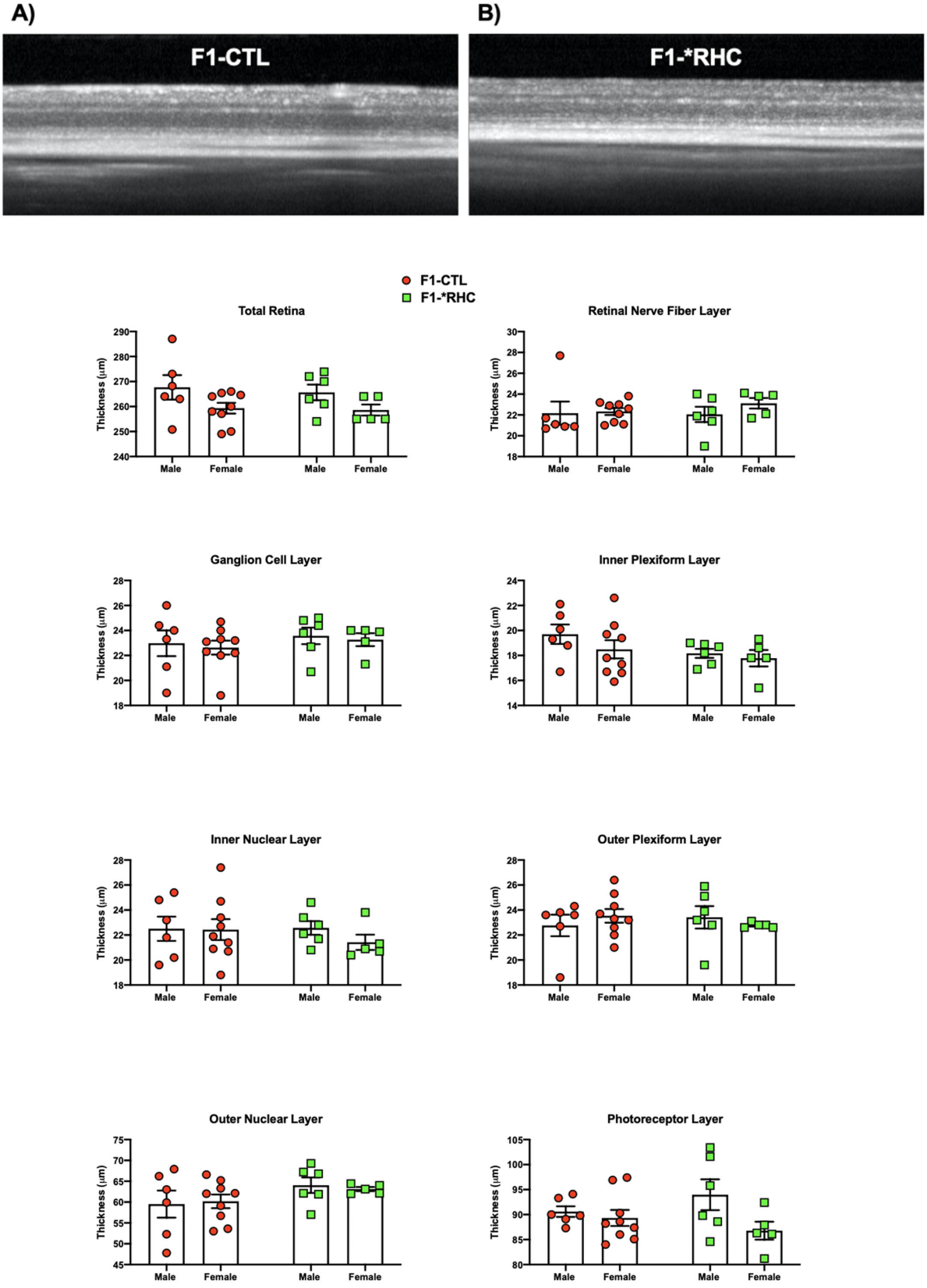

Figure 3. OCT of retinae from F1-CTL and F1-*RHC mice. F1 revealed no significant structural change in F1 retinae of either sex as a result of F0 parental RHC. Superior retina OCT scans from representative F1 mouse derived from control F0 parents (F1-CTL; 6 males, 9 females) **(A)** and F1 mouse derived from RHC-treated F0 parents (F1-*RHC; 6 males, 5 females) **(B)**. Remaining histograms show retinal layer thicknesses quantified over an 8.8-mm^2 circular area of the superior retina adjacent to the optic disc for each treatment group, by sex, with F1-CTL mice represented by *red circles* and F1-*RHC mice represented by *green squares*. Two-way ANOVA revealed no differences by treatment or sex for any layer.

Investigative Ophthalmology & Visual Science

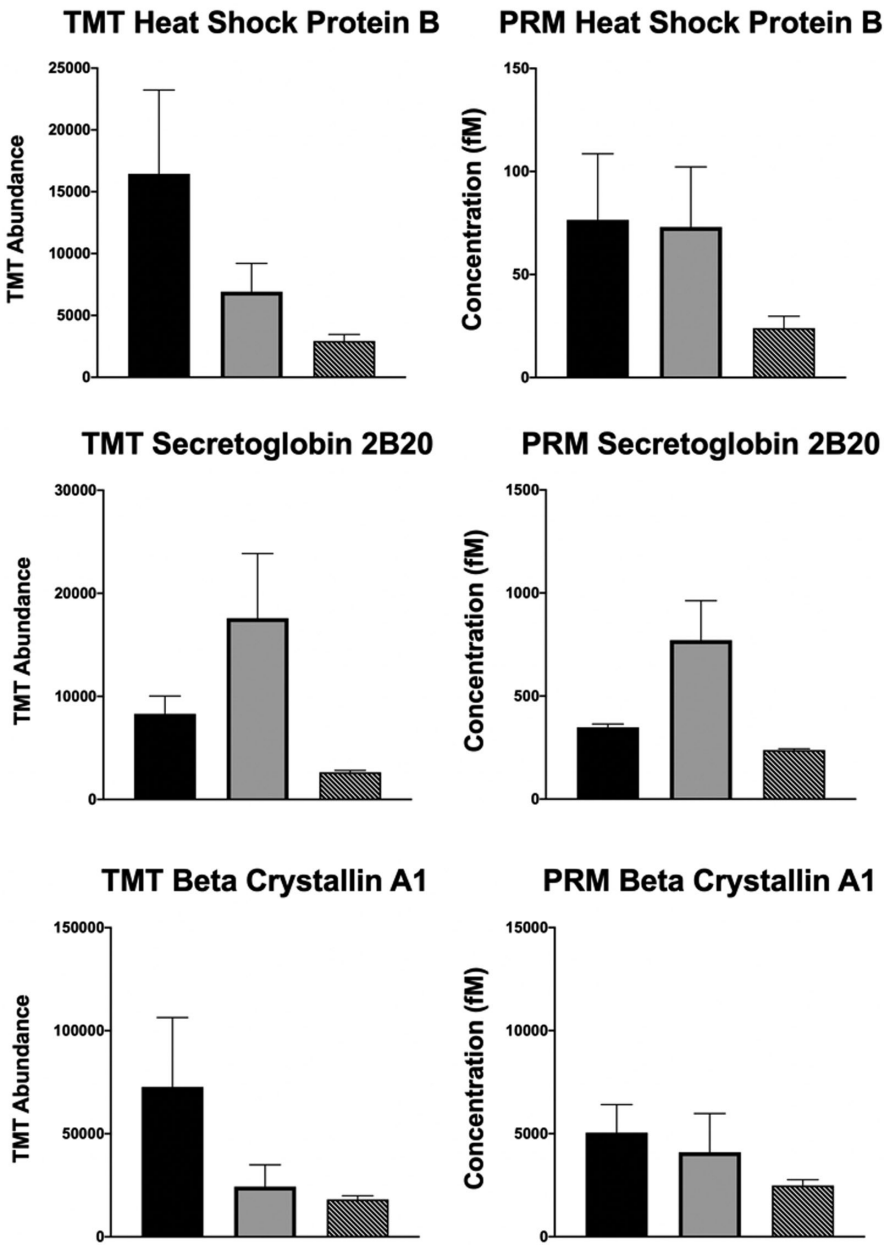

Figure 4. PRM validation of a sample proteomic dataset. TMT labels provided relative quantitation across groups, and PRM provided absolute quantitation. The data presented here represent the raw MS counts from samples obtained from the following experimental groups: F1 nonischemic retina from control F0 parents (*black*), F1 ischemic retina from control F0 parents (*gray*), and F1 ischemic retina from RHC-treated F0 parents (*hatched*). The TMT label abundance (*left column*) and respective PRM validation (*right column*) are displayed for the following three retinal proteins: heat shock protein B (*upper panel*), secretoglobin 2B20 (*middle panel*), and β-crystallin A1 (*lower panel*).

proteome of nonischemic retinae in control F1 mice derived from untreated parents (F1-CTL) (Fig. 1)—what we term the RHC ischemic response, or Comparison 2 (C2) (Table and Supplementary Table S1)—differed in many unique and significant ways from the aforementioned control ischemic response of F1 mice born to untreated F0 parents (C1). In total, 402 proteins were found to be significantly differentially expressed, with 314 exhibiting higher abundances, and 88 exhibiting lower abundances, relative to nonischemic retina. Moreover, 141 of the 314 differentially upregulated proteins and 42 of the 88 differentially downregulated proteins were not found to be differentially expressed in response to ischemia in untreated mice (the control ischemic response) (Supplementary Table S1).

Bioinformatic analyses of this RHC ischemic response revealed the top five enriched canonical pathways to be (1) CXCR4 signaling (11/167 proteins, $P = 2.2E\text{-}7$); (2) ephrin B signaling (7/72 proteins, $P = 2.8E\text{-}6$); (3) ephrin receptor signaling (10/180 proteins, $P = 3.7E\text{-}6$); (4) cardiac hypertrophy signaling (11/240 proteins, $P = 7.7E\text{-}6$); and (5) histamine degradation (4/17 proteins, $P = 1.2E\text{-}5$). The top five molecular and cellular functions were (1) cellular

Investigative Ophthalmology & Visual Science

Table. Top 20 Differentially Expressed Proteins (Abundance Ratios)

Comparison 1			Comparison 2			Comparison 3		
Gene ID	**Protein Name**	**FC Ratio**	**Gene ID**	**Protein Name**	**FC Ratio**	**Gene ID**	**Protein Name**	**FC Ratio**
Serpina3n	Serine protease inhibitor A3N	10.50	Ankrd54	Ankyrin repeat domain-containing protein 54	5.10	Hmgcs2	Hydroxymethylglutaryl-CoA synthase, mitochondrial	4.06
Fbln1	Fibulin-1	9.29	Comtd1	Catechol *O*-methyltransferase domain-containing protein 1	4.56	Krt14	Keratin, type I cytoskeletal 14	3.80
Serpina1d	Alpha-1-antitrypsin 1-4	6.89	Hist1h3i; Hist1h3a; Hist1h3g; Hist1h3h	Histone H3.1	4.03	Ankrd54	Ankyrin repeat domain-containing protein 54	3.63
Arg1	Arginase-1	6.16	Glycam1	Glycosylation-dependent cell adhesion molecule 1	3.97	Crygs	Beta-crystallin S	3.51
Cfb	Complement factor B	6.07	4933407H 18Rik; Uvssa	UV-stimulated scaffold protein A	3.87	Arhgef10	Rho guanine nucleotide exchange factor 10	3.40
Serpina3k	Serine protease inhibitor A3K	6.06	Dctn6	Dynactin subunit 6	3.71	Crybb1	Beta-crystallin B1	3.12
Igkc	Ig kappa chain C region	6.05	Slc24a4	Sodium/potassium/calcium exchanger 4	3.63	Grifin	Grifin	2.90
C1qa	Complement C1q subcomponent subunit A	5.82	Hmgcs2	Hydroxymethylglutar yl-CoA synthase, mitochondrial	3.45	Crybb2	Beta-crystallin B2	2.80
Serpina1b	Alpha-1-antitrypsin 1-2	5.69	Cabp5	Calcium-binding protein 5	3.43	Comtd1	Catechol Omethyltransferase domain-containing protein 1	2.73
Ces1c	Carboxylesterase 1C	5.55	Metap1	Methionine aminopeptidase 1	3.28	Slc2a13	Proton myo-inositol cotransporter	2.68
Cryge	Gamma-crystallin E	–11.24	Cryge	Gamma-crystallin E	–38.46	Serpina1b	Alpha-1-antitrypsin 1-2	–7.87
C030006K 11Rik	UPF0598 protein C8orf82 homolog	–6.41	Arl6ip1	ADP-ribosylation factor-like protein 6-interacting protein 1	–9.09	Serpina1a; Serpina1d	Alpha-1-antitrypsin 1-1	–7.64

Table. Continued

Comparison 1			Comparison 2			Comparison 3		
Gene ID	**Protein Name**	**FC Ratio**	**Gene ID**	**Protein Name**	**FC Ratio**	**Gene ID**	**Protein Name**	**FC Ratio**
Ppip5k1	Inositol hexakisphosphate/diphosphoinositolpentakisphosphate kinase 1	–6.06	Cryga	Gamma-crystallin A	–7.82	Mup11; Mup18; Mup2; Mup19	Major urinary protein 18	–7.30
Palm2	Paralemmin-2	–4.20	C030006K11Rik	UPF0598 protein C8orf82 homolog	–6.21	Serpina3k	Serine protease inhibitor A3K	–7.14
Crygd	Gamma-crystallin D	–4.18	Ppip5k1	Inositol hexakisphosphate and diphosphoinositol-pentakisphosphate kinase 1	–5.81	Tgfbi	Transforming growth factor-beta-induced protein ig-h3	–6.99
Thoc5	THO complex subunit 5 homolog	–4.12	Thoc5	THO complex subunit 5 homolog	–5.62	Arl6ip1	ADP-ribosylation factor-like protein 6-interacting protein 1	–6.58
Cwc15	Spliceosome-associated protein CWC15 homolog	–3.78	Tubb6	Tubulin beta-6 chain	–5.29	Ces1c	Carboxylesterase 1C	–6.58
Fabp5	Fatty acid-binding protein, epidermal	–3.48	1110037F02Rik; Virma	Protein virilizer homolog	–4.57	Serpina3n	Serine protease inhibitor A3N	–6.41
Grifin	Grifin	–3.46	Cwc15	Spliceosome-associated protein CWC15 homolog	–3.85	Alb	Serum albumin	–6.02
Bfsp2	Phakinin	–3.42	Slc25a46	Solute carrier family 25 member 46	–3.81	Apoa4	Apolipoprotein A-IV	–5.85

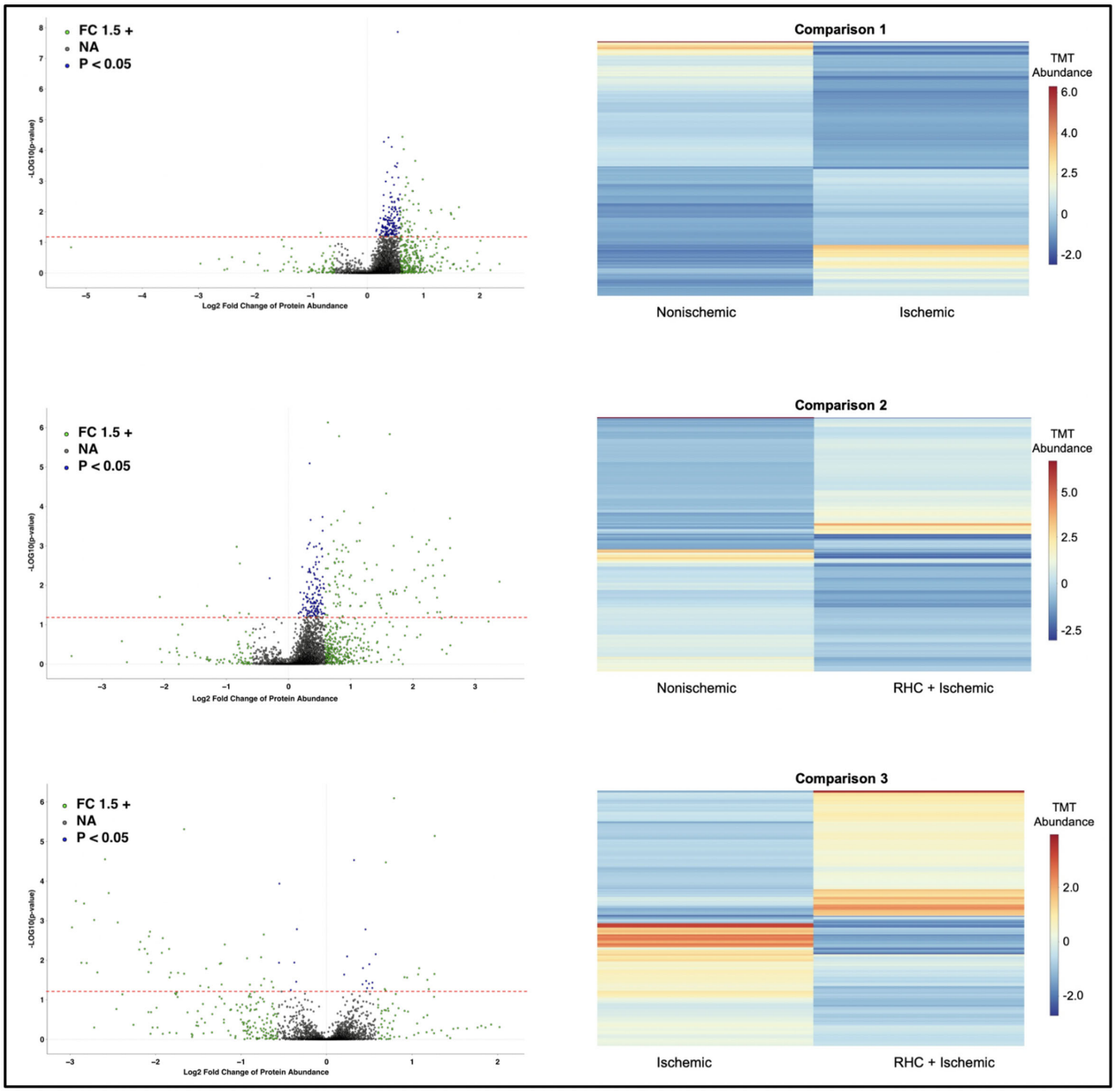

Figure 5. Volcano plots and heat maps revealed global differential protein expression by experimental comparison. Comparison 1 (*upper panels*): Ischemic retinae of F1 mice from normoxic (control) F0 parents relative to nonischemic retinae of F1 mice from normoxic (control) F0 parents. Comparison 2 (*center panels*): Ischemic retinae of F1 mice from hypoxic (RHC) F0 parents relative to nonischemic retinae of F1 mice from normoxic (control) F0 parents. Comparison 3 (*lower panels*): Ischemic retinae of F1 mice from hypoxic (RHC) F0 parents relative to ischemic retinae of F1 mice from normoxic (control) F0 parents. In the volcano plots (*left*), each point represents a unique protein, with its position on the plot based on the directional log2FC of each protein (*x*-axis) and the –log10(*P* value) (*y*-axis). Proteins in *green* were 1.5-fold or more abundant in that respective comparison. Proteins in *blue* are those with expression differences of $P < 0.05$ (above *dashed red line*) in that respective comparison. Proteins in *gray* are those that did not differ significantly in either fold-change or *P* value in that respective comparison. The heat maps (*right*) graphically display the differential expression, for each comparison, of the top 500 up- and downregulated proteins. The FC scale on the *y*-axis for each comparison is provided on the right; the *y*-axis shows upregulated proteins in *red* and downregulated proteins in *blue*. A maximum distance with complete linkage clustering method was applied, with data centered and scaled. Each row represents the abundance of a single protein.

assembly and organization (48 proteins, $P = 8.6E\text{-}3\text{–}1.2E\text{-}6$); (2) cellular function and maintenance (47 proteins, $P = 8.6E\text{-}3\text{–}1.2E\text{-}6$); (3) amino acid metabolism (14 proteins, $P = 7.2E\text{-}3\text{–}3.8E\text{-}6$); (4) small molecule biochemistry (43 proteins, $P = 8.6E\text{-}3\text{–}3.8E\text{-}6$); and (5) cell-to-cell signaling and interaction (35 proteins, $P = 8.6E\text{-}3\text{–}6.6E\text{-}5$). The top five upstream regulators of the RHC ischemic response were (1) TP53 ($P = 1.1E\text{-}5$); (2) amyloid beta precursor protein

Investigative Ophthalmology & Visual Science

(P = 3.1E-5); (3) cytochrome P450 oxidoreductase (P = 2.1E-4); (4) mitogen-activated protein kinase-1 (P = 3.4E-4); and (5) microRNA miR-1228-5p (P = 3.8E-4).

It is clear that, at the level of individual proteins and pathways, parental RHC fundamentally changed the response to ischemia in their offspring. None of the top five canonical pathways was shared between C1 and C2, and the only top five upstream regulator they had in common was TP53. With respect to the top five molecular and cellular functions, only the cellular assembly and organization pathway and the cell-to-cell signaling and interaction pathway were shared.

To further probe these datasets, we performed additional bioinformatic analyses of only the proteins that were differentially expressed in C1 but not C2, as well as, conversely, only the proteins that were differentially expressed in C2 but not C1. Omitting from the analysis the proteins that were differentially expressed in one comparison but not the other provided more mechanistic insights into each response while also providing additional confirmation of the original findings for each comparison despite the inclusion of redundant proteins. In terms of the IPA core analyses and the proteins that were only differentially expressed in C1 but not in C2, the top 5 canonical pathways were (1) acute phase response signaling (23/179 proteins, P = 7.5E-18); (2) LXR/RXR activation (15/121 proteins, P = 7.8E-12); (3) FXR/RXR activation (15/126 proteins, P = 1.4E-11); (4) coagulation system (9/35 proteins, P = 1.4E-10); and (5) actin cytoskeleton signaling (13/218 proteins, P = 1.3E-6). In turn, the top five molecular and cellular functions were (1) protein synthesis (63 proteins, P = 2.5E-5–1.1E-16); (2) cellular movement (105 proteins, P = 5.9E-5–2.8E-16); (3) cellular compromise (41 proteins, P = 1.1E-05–1.2E-13); (4) free radical scavenging (35 proteins, P = 1.6E-5–7.3E-13); and (5) molecular transport (86 proteins, P = 5.1E-5–2.4E-11). Finally, the top five upstream regulators were (1) TGF-β1 (P = 9.9E-15); (2) Hmgn3 (P = 1.8E-12); (3) PRL (P = 4.6E-12); (4) TP53 (P = 3.4E-10); and (5) cell proliferation regulator and Ras-based GTPase KRAS (P = 4.0E-10). Of note, four out of five canonicals, three out of five molecular and cellular functions, and four out of five upstream regulators were identical, even after removing the 220 proteins from the C1 dataset that were not differentially expressed in C2.

With respect to the proteins that were only differentially expressed in C2 but not in C1, the top 5 canonical pathways were (1) endocannabinoid developing neuron pathway (6/115 proteins, P = 2.5E-4); (2) CXCR4 signaling (7/167 proteins, P = 2.9E-4); (3) antiproliferative role of somatostatin receptor 2 (5/77 proteins, P = 3.0E-4); (4) ephrin receptor signaling (7/180 proteins, P = 4.5E-4); and (5) BMP signaling pathway (5/85 proteins, P = 4.7E-4). The top five molecular and cellular functions were (1) cell-to-cell signaling and interaction (33 proteins, P = 8.1E-3–5.2E-5); (2) amino acid metabolism (9 proteins, P = 7.6E-3–5.6E-5); (3) small molecule biochemistry (40 proteins, P = 8.1E-3–5.7E-5); (4) cellular development (46 proteins, P = 8.6E-3–5.7E-5); and (5) molecular transport (46 proteins, P = 8.1E-3–1.6E-4). The top five upstream regulators of the RHC ischemic response were (1) TP53 (P = 6.0E-6); (2) microRNA miR-450b-3p (P = 5.4E-5); (3) cytochrome P450 oxidoreductase (P = 9.6E-5); (4) DNA-binding homeobox protein EN1 (P = 1.3E-4); and (5) paired box transcription factor family member PAX3 (P = 1.72E-4). In this case, removing the 219 proteins from C2 that were not differentially expressed in C1 yielded three out of five new top-ranked canonicals, two out of five new molecular and cellular functions, and three out of five new upstream regulators.

Two Distinct Postischemic Retinal Proteomes—Comparison 3

Directly comparing the postischemic retinal proteome of mice from RHC-treated parents (F1-*RHC) to that of mice from untreated parents (F1-CTL) (Fig. 1)—which we term the RHC versus control ischemic response, or Comparison 3 (C3) (Table and Supplementary Table S1)—provides another distinct way to probe the mechanistic basis of the ischemia-resilient phenotype. In total, 266 proteins were found to be significantly differentially expressed in this dataset, with 73 proteins exhibiting higher abundances and 193 proteins exhibiting lower abundances (Table and Supplementary Table S1). These differences support the general conclusion that, at the time point examined, parental RHC results in an overall suppression of ischemia-induced changes in protein expression. Many of these downregulated proteins (e.g., integrins, G-protein-coupled receptors, receptor tyrosine kinases) serve as molecular switches that activate or inhibit signaling pathways. The top five canonicals representing this comparison were (1) acute phase response signaling (22/179 proteins, P = 6.9E-22); (2) LXR/RXR activation (16/121 proteins, P = 1.1E-16); (3) FXR/RXR activation (16/126 proteins, P = 2.0E-16); (4) coagulation system (9/35 proteins, P = 1.1E-12); and (5) complement system (6/37 proteins, P = 1.4E-7). The top five molecular and cellular functions defining C3 were (1) cellular compromise (39 proteins, P = 1.3E-4–1.4E-17); (2) cellular movement (69 proteins, P = 1.3E-4–2.6E-15); (3) protein synthesis (44 proteins, P = 1.3E-4–9.8E-15); (4) lipid metabolism (56 proteins, P = 1.3E-4–1.6E-11); and (5) molecular transport (60 proteins, P = 1.3E-04–1.6E-11). Finally, the top five upstream regulators for this RHC versus control ischemia comparison were (1) Hmgn3 (P = 6.3E-15); (2) TP53 (P = 2.4E-13); (3) PRL (P = 9.5E-13); (4) IL-6 (P = 3.2E-12); and (5) the photoreceptor-specific transcription factor known as cone–rod homeobox protein (P = 2.6E-10).

We performed a comparison analysis of the differentially expressed proteins across all three experimental groups/comparisons, and, based on activation z-scores, which are used to predict activation or inhibition, where scores of $\geq\pm2$ identical to $\geq\pm2$ standard deviations (95% confidence) are indicative of statistical significance, we ranked the top 30 canonical pathways, upstream regulators, and molecular and cellular (biological) functions as variables (Fig. 6). Examination of the z-score-based heat map values for a given pathway, regulator, and function revealed many, often very robust, differences among the three experimental groups/comparisons. For example, an upregulation of canonical integrin signaling defined the response to ischemia in the control mice (C1) but less so in the *RHC mice (C2), to the extent that, when comparing ischemic retinae from the two groups directly to one another (RHC vs. control ischemia, C3), the overall reduction in integrin signaling that occurs in the ischemic retina as a result of parental RHC became evident. The same conclusion applies to the canonical signaling pathways for synaptogenesis, Rho family GTPases, actin cytoskeleton, Rac, LXR/RXR activation, paxillin, leukocyte extravasation, acute-phase response, cell division cycle 42 (CDC42), Nrf2, and RhoA, to name a few. It is also important to point out that identifying the top

Investigative Ophthalmology & Visual Science

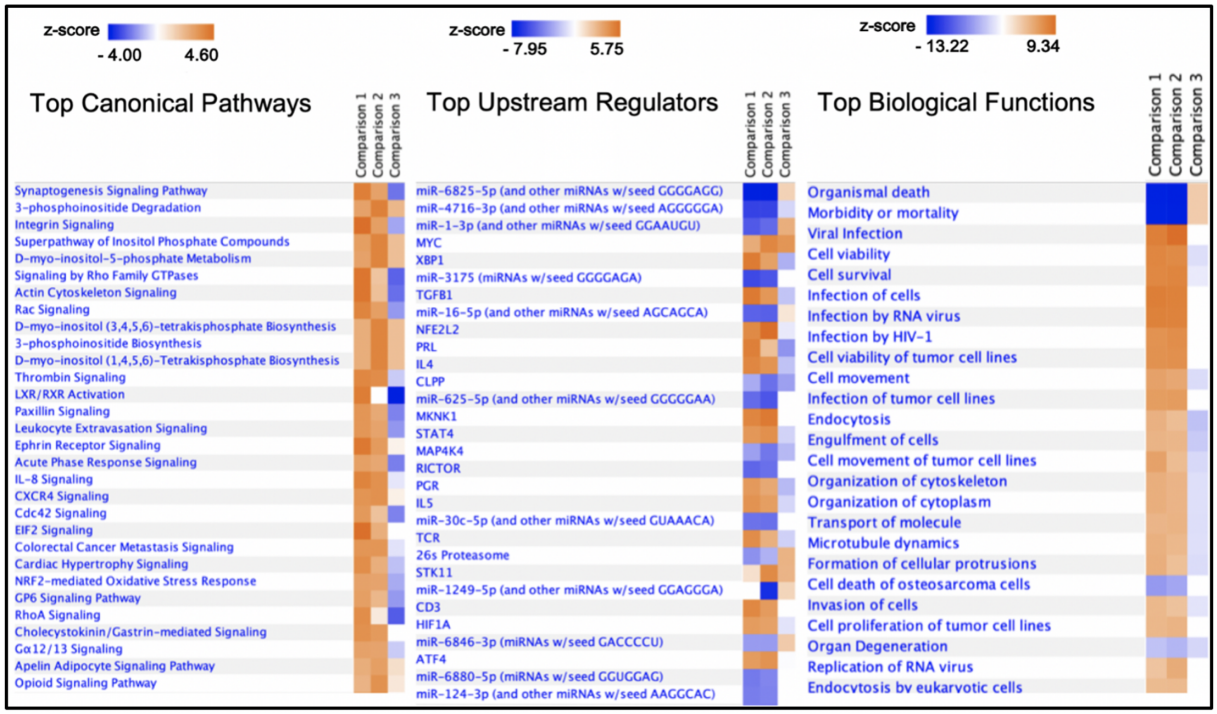

Figure 6. Top canonical pathways, upstream regulators, and biological functional enrichments, by experimental comparison. IPA core analyses were performed for each of the three individual comparisons, and then an IPA comparison analysis was run among all three comparisons to yield the most enriched canonical pathways (*left*), upstream transcriptional regulators (*center*), and biological/molecular functions (*right*), with *z*-score-based heat maps for each pathway, regulator, and function. Only canonicals with a *z*-score of greater than ±2.0 (= 95% confidence interval) are shown. Positive z-scores (*orange*) indicate activation/upregulation of the pathway, and negative *z*-scores (*blue*) indicate suppression/downregulation of the pathway, for each comparison.

canonicals and other pathways/networks for a given dataset does not concomitantly provide information about the directional changes of the differentially expressed proteins therein. But, these comparison analyses (Fig. 6) do just that. As examples, acute-phase response (APR) signaling was identified as the highest ranked canonical for both C1 and C3, but a comparison analysis revealed that, overall, the expression of many proteins comprising this pathway—as well as the LXR/RXR activation, FXR/RXR activation, and coagulation system pathways—were robustly upregulated in F1-CTL mice, whereas in F1-*RHC mice the expression of the majority of proteins in the same respective pathways was robustly downregulated.

In addition to probing the upstream regulators predicted to be driving the observed expression changes and the downstream biological functions they influence, protein-specific insights into the mechanisms by which parental RHC augments retinal resilience in their offspring can also be gleaned from bioinformatically probing the differentially expressed proteins that comprise a given canonical pathway or biological function. Doing this for each of the three experimental comparisons that define our study—including taking into account the magnitude of the respective protein expression changes therein, the location of these differentially expressed proteins in the respective pathway/network, their functional relationship to other differentially expressed proteins, and the respective direction of their expression changes—provided insights into the mechanistic basis of intergenerational protection. Below are three examples from many that we derived from such deeper analyses.

Visual Phototransduction

The process of converting photons of light into an electrical signal in the retina, known as visual phototransduction, is what we recorded noninvasively in control and *RHC mice by scotopic (dark-adapted) flash electroretinography; we subsequently quantified at distinct flash intensities the a-wave and b-wave components of the resultant mass potential, which originate from the activity of photoreceptors and cells of the inner retina, respectively, as functional metrics of retinal ischemic injury and resilience (Fig. 2). Our MS analysis of ischemic retinae from F1 control mice (C1) and F1-*RHC mice (C2) revealed many rod-specific proteins that, relative to nonischemic retinae, were differentially expressed in each cohort (Fig. 7), thereby providing a molecular basis for the epigenetically mediated functional protection we documented. As evident in the figure, its companion heat map, and the companion table of expression differences for the proteins that comprise the canonical, by comparison the control ischemic response (C1) (Fig. 7, upper panel) is defined by a significant, 2.5-fold reduction in rhodopsin expression (as well as a 1.5-fold reduction in short-wave-sensitive opsin-1), a 1.5-fold reduction in regulator of G-protein signaling 9-binding protein expression, and a 1.2-fold reduction in G protein subunit alpha transducin 1 (GNAT1) expression (the subunit that contains the GTP binding site), relative to nonischemic retinae. Also defining this response are 1.6- and 1.8-fold increases in the expression of transducin-β subunits GNB1 and GNB3 (the subunits regulating GTPase activity), and a 1.3-fold increase in S-arrestin.

Investigative Ophthalmology & Visual Science

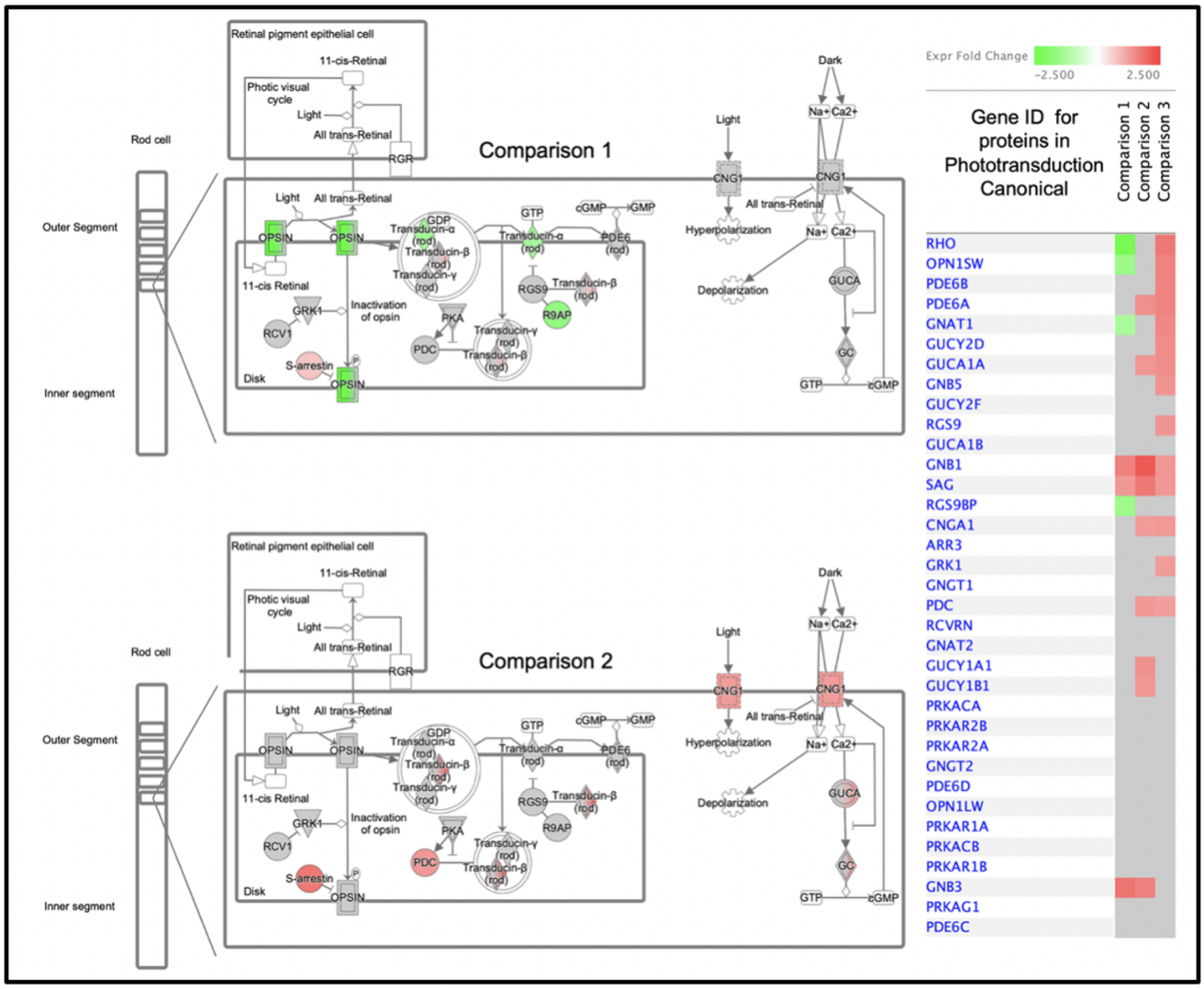

		Comparison 1		Comparison 2		Comparison 3	
Gene	**Protein ID**	**Fold Change**	**p-value**	**Fold Change**	**p-value**	**Fold Change**	**p-value**
CNGA1	cyclic nucleotide gated channel subunit alpha 1	-	-	1.266	0.476	1.304	0.259
GNAT1	G protein subunit alpha transducin 1	-1.235	0.49	-	-	1.519	0.0969
GNB1	G protein subunit beta 1	1.629	0.177	2.175	0.00915	1.335	0.482
GNB3	G protein subunit beta 3	1.8	0.0814	1.628	0.123	-	-
GNB5	G protein subunit beta 5	-	-	-	-	1.371	0.468
GRK1	G protein-coupled receptor kinase 1	-	-	-	-	1.267	0.336
GUCA1A	guanylate cyclase activator 1A	-	-	1.33	0.203	1.45	0.0366
GUCY1A1	guanylate cyclase 1 soluble subunit alpha 1	-	-	1.385	0.307	-	-
GUCY1B1	guanylate cyclase 1 soluble subunit beta 1	-	-	1.329	0.172	-	-
GUCY2D	guanylate cyclase 2D, retinal	-	-	-	-	1.461	0.35
OPN1SW	opsin 1, short wave sensitive	-1.49	0.158	-	-	1.602	0.0534
PDC	phosducin	-	-	1.321	0.263	1.235	0.486
PDE6A	phosphodiesterase 6A	-	-	1.426	0.404	1.558	0.22
PDE6B	phosphodiesterase 6B	-	-	-	-	1.558	0.413
RGS9	regulator of G protein signaling 9	-	-	-	-	1.359	0.48
RGS9BP	regulator of G protein signaling 9 binding protein	-1.462	0.282	-	-	-	-
RHO	rhodopsin	-2.481	0.0335	-	-	1.746	0.247
SAG	S-antigen visual arrestin	1.32	0.215	1.745	0.00209	1.322	0.15

Figure 7. Parental RHC reverses ischemia-induced changes in rod phototransduction pathway proteins. Displayed is the IPA version of the phototransduction canonical pathway for Comparison 1 (*upper panel*) and Comparison 2 (*lower panel*) (see Supplementary Fig. S2 for Comparison 3 for this same canonical). Proteins and their isoforms responsible for generating an electrical response to light are arranged anatomically relative to the rod outer segment (the section of the photoreceptor containing disks full of the photosensitive pigment rhodopsin and other molecules involved in the visual transduction process), as well as the channels and molecular mediators of the so-called dark

Investigative Ophthalmology & Visual Science

current that maintain the rod in a depolarized state in the absence of light. The heat map shows the directional FC, by comparison, for each protein in the canonical, ranked by expression FC for C1. Note that many of the proteins that are downregulated (*green*) in the ischemic retinae of F1 mice from control parents (Comparison 1) are either no longer downregulated or even upregulated (*red*) in the ischemic retinae of F1 mice from RHC-treated parents (Comparison 2). A tabulated version of this canonical is provided with the fold changes and *P* values for each protein in the canonical and each respective comparison.

In contrast, the RHC ischemic response (C2) (Fig. 7, lower panel) reveals in striking fashion how the rod proteome was completely modified by parental RHC. No longer are the aforementioned downregulated proteins affected; rather, the expression of one of these is now upregulated (GNAT1, by 1.2-fold), and the expression of several other photoreceptor proteins that were unaffected by ischemia are now significantly upregulated: specifically, phosphodiesterase 6 (PDE6) α-subunit by 1.4-fold and the phosphoprotein phosducin by 1.3-fold. Of note, the ischemia-induced increases in transducin-β and S-arrestin expression were significantly increased in *RHC mice, even more so than in untreated mice, consistent with the notion that augmenting their expression may be an endogenous response on the part of the rods to counter the deleterious effects of ischemia and that RHC is facilitating this response. Moreover, the ischemic photoreceptors of *RHC mice exhibited a significantly greater expression of several proteins regulating the dark current, including a 1.3-fold increase in the alpha subunit of the cGMP-gated cation channel protein and 1.3-fold increases in the calcium-sensitive guanylate cyclase activating protein 1A and 1B, as well as 1.4- and 1.3-fold increases in the α1 and β1 subunits, respectively, of soluble guanylate cyclase. None of these expression changes occurred in the ischemic photoreceptors of control mice (C1).

Comparing control ischemic retinae directly to *RHC ischemic retinae (C3) (Supplementary Fig. S2) reveals that 13 proteins in the visual transduction pathway of rod photoreceptors were expressed at levels 1.2-fold or greater between the two phenotypes, including rhodopsin kinase and the transducing α-binding regulator of G-protein signaling 9 (RGS9). Because some of these (i.e., the transducins and guanylate cyclase) are enzymes, treatment-induced changes in their abundance of more than 20% suggest a very substantial modulation in visual transduction cycle function.

Actin Cytoskeleton Signaling

Shown in Figure 8 is the actin cytoskeleton signaling network canonical for C3, along with a heat map that displays how each protein in the network was affected under all three experimental conditions (C1–C3). When analyzed in conjunction with the corresponding networks for C1 and C2 (Supplementary Fig. S3, upper and lower panels, respectively), it becomes clear how the signaling responsible for ischemia-triggered polymerization and destabilization of actin, as well as the assembly of focal adhesions and complexes, was countered by parental RHC.

Mechanistically, the expression changes we measured predict that these pathological changes are attenuated, neutralized, or even reversed in the ischemic retinae of *RHC mice as a result of overall increases in the postischemic expression of integrin subunit β1 (by 1.4-fold), RhoA (by 1.9-fold), the adaptor protein BAIAP2 (by 1.2-fold), and the adhesion/contact proteins paxillin and talin 1 (by 2.3-fold and 1.3-fold, respectively). Concomitantly, RHC led to overall decreases in the postischemic expression of several components of the actin-related protein 2/3 complex, including actin-related binding proteins 2 and 3 (ARP2 and ARP3) and subunit 1B (ARPC1B), as well as the actin-binding protein filamin-A; spectrin family protein actinin alpha 4 (by 1.3-fold); adherens junction-forming Ras GTPase-activating-like protein IQGAP1 (by 1.4-fold); adhesion contact protein profilin 2 (by 1.3-fold); F-actin binding protein vinculin; and actin filament organizing protein cofilin (CFL1 and CFL2, by 1.2- and 1.3-fold, respectively). Additional effectors of the RHC-protective phenotype include reductions in the expression of filamentous actin (F-actin) and several myosin light chain (MLC) isoforms, as well as much lower circulating levels of fibronectin (FN1), thrombin, and kinogens such as bradykinin that drive cytoskeletal pathobiology. Other top canonicals (Fig. 6) related to cytoskeletal dynamics, and which exhibit contrasting activation/inhibition for C1/C3, include RhoA signaling, Rac signaling, CDC42 signaling, paxillin signaling, and integrin signaling. Similarly, the related top biological functions (Fig. 6) include cell movement, organization of cytoskeleton, organization of cytoplasm, microtubule dynamics, and formation of cellular protrusions. In addition, directionally similar and statistically significant expression changes were also observed with respect to RHC-associated decreases in ARP2/3, IQGAP1, ERM proteins (ezrin, radixin, and moesin), MLC, and CFL in two other related canonicals—RhoGTPase family and RhoGDI signaling—for C3 (data not shown), all of which underscore the critical role these cytoskeleton proteins likely play in manifesting the ischemia-resilient phenotype.

Acute Phase Response Signaling

Figure 9 shows the differentially expressed proteins participating in the APR for the RHC-to-control ischemic response comparison (C3), again alongside a companion heat map showing how each protein in the pathway was affected across all three experimental conditions and comparisons. Also provided in tabular form are the fold changes and respective *P* values for the expression differences of all of the proteins in the canonical, sorted by comparison. Note the robust downregulation of almost all of the major proteins comprising this particular response to ischemia as a result of parental RHC, including a 3.1- to 3.8-fold downregulation of the A1, A2, and H apolipoprotein transporters; a 4.4-fold downregulation in transthyretin expression (which, among other functions, transports retinol, or vitamin A, in the plasma by associating with retinol binding-proteins); a 1.9- to 5.2-fold downregulation in the levels of the plasma protease regulators alpha-2-HS-glycoprotein, alpha-2-macroglobulin, and hemopexin [HPX], a 3.5- to 4.8-fold downregulation in selected complement factors (CFB, C3, and C9); and a 1.7- to 4.2-fold downregulation in selected coagulation and extracellular matrix regulators, including fibronectin (FN1), plasminogen, prothrombin, and the alpha, beta, and gamma subunits

Investigative Ophthalmology & Visual Science

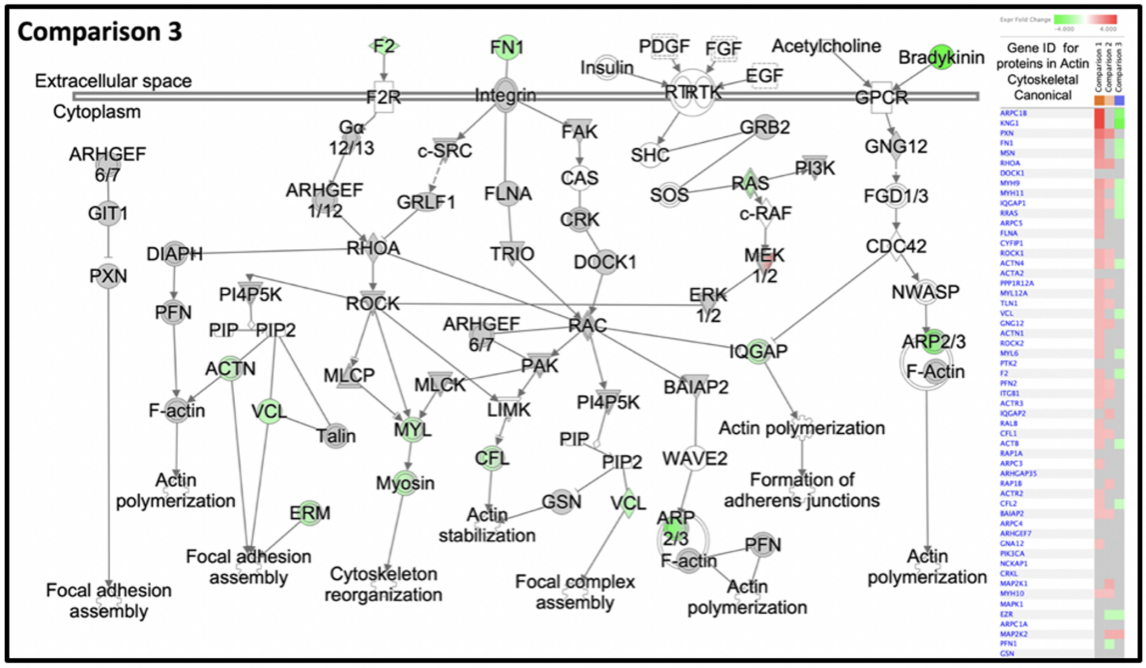

Gene	Protein ID	Comparison 1 Fold Change	Comparison 1 p-value	Comparison 2 Fold Change	Comparison 2 p-value	Comparison 3 Fold Change	Comparison 3 p-value
ACTB	actin beta	1.35	0.0390	-1.21	0.2820	-	-
ACTN1	actinin alpha 1	1.45	0.2180	-	-	-	-
ACTN4	actinin alpha 4	1.55	0.0000	-1.27	0.0016	1.22	0.0090
ACTR2	actin related protein 2	1.31	0.3310	-	-	-	-
ACTR3	actin related protein 3	1.39	0.1210	-	-	-	-
ARPC1B	actin related protein 23 complex subunit 1B	4.35	0.1800	-2.86	0.3670	-	-
ARPC3	actin related protein 23 complex subunit 3	1.34	0.1010	-	-	-	-
ARPC5	actin related protein 23 complex subunit 5	1.67	0.4070	-	-	-	-
BAIAP2	BARIMD domain containing adaptor protein 2	1.29	0.2810	-	-	1.24	0.4340
CFL1	cofilin 1	1.37	0.0019	-	-	1.29	0.0152
CFL2	cofilin 2	1.30	0.0592	-	-	-	-
EZR	ezrin	-	-	-1.35	0.1530	-1.36	0.2380
F2	coagulation factor II, thrombin	1.44	0.3540	-1.50	0.2650	-	-
FLNA	filamin A	1.65	0.1710	-	-	-	-
FN1	fibronectin 1	2.23	0.0340	-1.74	0.1150	-	-
GNA12	G protein subunit alpha 12	1.26	0.2390	-	-	-	-
GNG12	G protein subunit gamma 12	1.46	0.4690	-	-	1.44	0.4830
IQGAP1	IQ motif containing GTPase activating protein 1	1.76	0.0051	-1.40	0.1090	1.26	0.4890
IQGAP2	IQ motif containing GTPase activating protein 2	-	-	-	-	1.51	0.1320
ITGB1	integrin subunit beta 1	1.42	0.0098	-	-	1.36	0.0193
KNG1	kininogen 1	4.06	0.0040	-4.22	0.0025	-	-
MAP2K1	mitogen-activated protein kinase kinase 1	-	-	-	-	1.64	0.2100
MAP2K2	mitogen-activated protein kinase kinase 2	-	-	1.65	0.1660	1.62	0.2270
MSN	moesin	2.10	0.2160	-1.58	0.4950	-	-
MYL6	myosin light chain 6	1.44	0.1590	-1.35	0.3830	-	-
MYH9	myosin heavy chain 9	1.90	0.0011	-1.38	0.1520	1.38	0.1310
MYH10	myosin heavy chain 10	1.22	0.0420	-	-	1.24	0.0173
MYH11	myosin heavy chain 11	1.77	0.0677	-1.47	0.4370	-	-
MYL12A	myosin light chain 12A	1.48	0.1070	-	-	-	-
PFN1	profilin 1	-	-	-	-	-1.28	0.2660
PFN2	profilin 2	1.42	0.0175	-	-	1.27	0.1380
PPP1R12A	protein phosphatase 1 regulatory subunit 12A	1.49	0.1100	-	-	1.26	0.3760
PXN	paxillin	2.76	0.0172	-	-	2.25	0.0621
RALB	RAS like proto-oncogene B	1.38	0.1200	-	-	-	-
RAP1B	RAP1B, member of RAS oncogene family	-	-			1.34	0.4890
RHOA	ras homolog family member A	1.98	0.0063	-	-	1.88	0.0090
ROCK1	Rho associated coiled-coil containing protein kinase 1	1.56	0.0016	-	-	1.31	0.0276
ROCK2	Rho associated coiled-coil containing protein kinase 2	1.44	0.1560	-	-	-	-
RRAS	RAS related	1.73	0.0294	-1.47	0.1520	-	-
TLN1	talin 1	1.47	0.0117	-	-	1.26	0.1980
TLN2	talin 2	-	-	-	-	1.25	0.1900
VCL	vinculin	1.47	0.0640	-1.38	0.1470	-	-

Figure 8. Parental RHC suppresses postischemic actin cytoskeleton signaling in F1 retinae. Axon guidance, cell motility, and a myriad of other important cellular functions are directed by actin remodeling. This complex regulatory signaling is directed by many members of the Rho family of small GTPases. Displayed is the IPA actin cytoskeleton signaling pathway for Comparison 3 (see Supplementary Fig. S3 for Comparisons 1 and 2 for this same canonical), with differentially expressed proteins colored *red* (upregulated) or *green* (downregulated), based on FC. The heat map shows the directional FC, by comparison, for each protein in the canonical, ranked by expression FC for C1. Note

that many of the same proteins that are upregulated in mice from untreated parents (*shades of red*, Comparison 1; *red-gray*, Comparison 2) are downregulated in mice from RHC-treated parents (*shades of green*, Comparison 3). A tabulated version of this canonical is provided with the fold changes and *P* values for each protein in the canonical and each respective comparison.

of fibrinogen. Of note, FN1, which serves as a ligand for integrin membrane receptors that modulate actin cytoskeleton signaling and remodeling, in addition to playing a role in protein chaperoning, binding, and cell activation in the plasma, differed in expression nearly fourfold between C1 and C3. Additionally, we found a 2.4- to 7.9-fold downregulation in the selected serine protease inhibitors α1-antitrypsin (SERPINA1), α1-antichymotrypsin (SERPINA3), and heparin cofactor 2 (SERPIND1). Conversely, the expression of MnSOD, the mitochondrial enzyme that clears superoxide and thus plays a central role combating ischemia-related oxidative stress and a proinflammatory cytokine burden, was upregulated in the F1-*RHC ischemic retina. These changes contrast with those defining the control ischemic response for this pathway (C1, Supplementary Fig. S4, upper panel), which is characterized by the robust, 2- to 10-fold, significant upregulation of all of these same pathway proteins (except SERPINA1), as well as others in this canonical, secondary to increases in upstream glucocorticoid receptor activation, p38MAPK, and Rac. In turn, the effect of parental RHC (C2) is so robust with regard to inhibiting this overall response systemically that, bioinformatically speaking, the acute phase response does not register as activated (Supplementary Fig. 4, lower panel), and none of the APR pathway proteins exhibited significant changes in these retinae at 10 days postischemia. The following specific molecular example underscores how robustly parental RHC dampened the APR when using C3 as a reference. The proinflammatory cytokine TGF-β1, which was identified as one of the top-ranking upstream regulators in C1 with a *z*-score of 5.3, was expressed at nearly sevenfold lower levels in C3 (*z*-score of –1.8), a difference that was also confirmed by our MS results with respect to protein abundance. Additional differences in immune-related protein expression between C1 and C3 are also evident as heat map differences for a number of biological functions listed in Figure 9, including cellular mobilization, cell invasion, and endocytosis/engulfment of cells.

Discussion

Evidence supporting the nongenetic inheritance of disease susceptibility as a result of adverse stress-induced epigenetic modifications to the parental germline continues to grow.[6–11] Results of the present study juxtapose these findings by showing for the first time, to the best of our knowledge, that exposure of adult mice to repetitive systemic hypoxia during adulthood—and prior to conception—protects against retinal ischemic injury in their adult F1-generation progeny. Thus, not only can disease burden be inherited across generations as a result of maladaptive responses on the part of parents, but progeny can also inherit disease resilience secondary to adaptive responses on the part of their parental lineage to beneficial stress stimuli that promote such phenotypes. To our knowledge, this is the first report of the intergenerational inheritance of an induced phenotype that protects against injury in mammals or even vertebrates. Other studies in rodents have demonstrated a behavioral flexibility in F1 offspring derived from F0 fathers that were subjected to maternal separation and stress during their first 2 weeks of postnatal life,[32] as well as improvements in memory metrics in offspring from parents exposed to mentally and physically enriched environments.[33,34] However, although they serve as examples of the inheritance of beneficial phenotypes, these intergenerationally modified phenotypes were not ones that protected against injury per se.

Whether disease or health phenotypes induced in parents secondary to environmental stress or change are passed to their immediate or even multiple generations, at least four primary mechanisms orchestrate this entire process, each of which presents fundamental biological questions. Taken in order, the first question is how does systemic, environmental stress ultimately lead to germ cell reprogramming? Second, what epigenetic modifications or marks are responsible for germ cell DNA modifications that survive what was long believed to be full erasure of such marks upon fertilization? The manner in which these epigenetic marks in the zygote coordinate the ultimate differentiation of maladaptive or adaptive phenotypes in the adult, in the absence of any ecological and cultural influences on inheritance, and how these phenotypes are maintained across the lifespan represent the third sequential component of this larger mystery. Finally, what are the tissue- and even cell-specific molecular signatures of these modified phenotypes? Gaining a working-level knowledge base for each of these mechanisms will take decades of concerted, interdisciplinary research. That said, as a first step toward gaining a foothold on one of these unanswered questions, we sought to leverage the breadth and depth of proteomics to begin to understand how disease resilience, which we documented at the functional level by electroretinography, is manifested phenotypically in the retina of F1-*RHC mice. For this particular question, such knowledge also carries significant therapeutic implications.

Predictably, the retinal proteome of these protected F1 animals was strikingly distinct from that of their matched, untreated controls, even down to the level of photoreceptor visual transduction proteins subunits. Not only did we identify hundreds of differentially expressed, up- and downregulated proteins and protein subunits by name, but our extensive bioinformatics analyses also revealed myriad biochemical pathways and networks in which they participate that were modified in the ischemic F1 retina as a result of parental RHC, including diverse signaling and metabolic pathways not typically associated with neuroprotection. Such levels of endogenous plasticity in a mature tissue would be considered impressive if uncovered in one directly exposed to a particular therapeutic, but we cannot emphasize enough that the phenotypic changes we documented herein were inherited secondary to parental treatment. We provided herein extensive lists of both the proteins and the key molecular pathways in which they participate with respect to both injury (C1) and protection (C2), including likely upstream regulators and downstream effectors. We also examined the RHC-induced, ischemia-resilient phenotype from the dual perspectives of how it differs from the nonischemic phenotype (C2) and how it differs from the

Investigative Ophthalmology & Visual Science

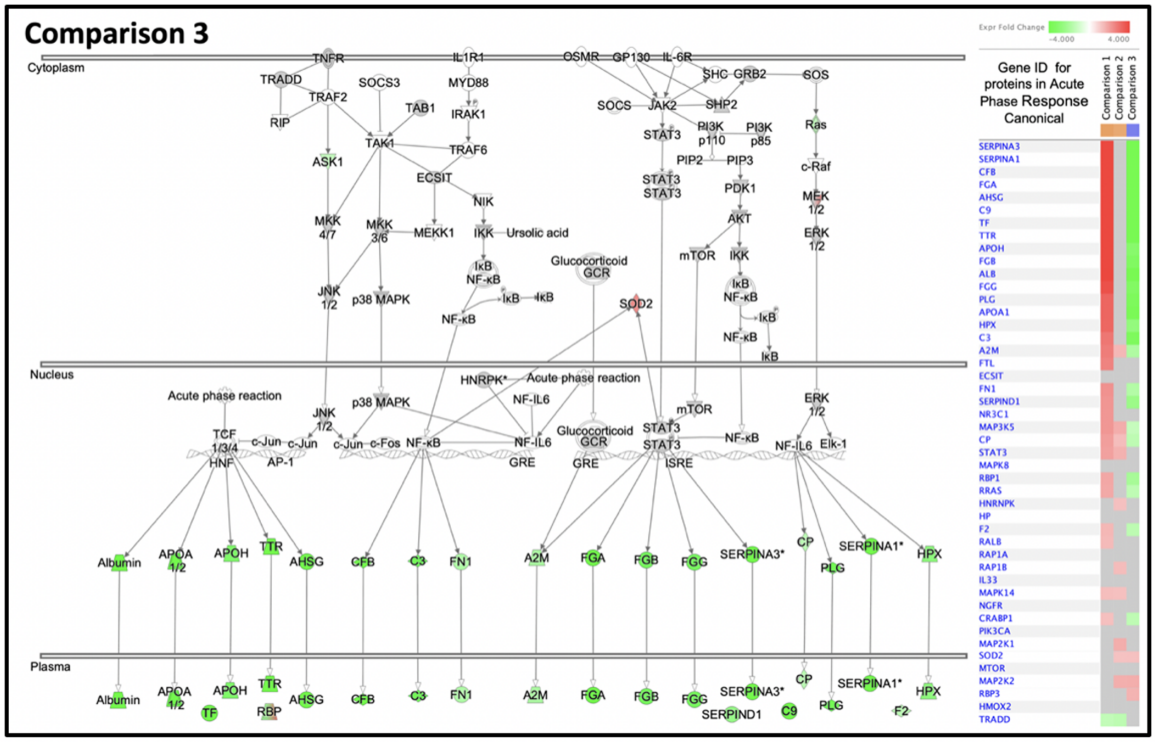

		Comparison 1		Comparison 2		Comparison 3	
Gene	**Protein ID**	**Fold Change**	**p-value**	**Fold Change**	**p-value**	**Fold Change**	**p-value**
A2M	alpha-2-macroglobulin	2.67	0.0030	1.45	0.4310	-1.85	0.0847
AHSG	alpha 2-HS glycoprotein	5.42	0.0480	-	-	-5.24	0.0727
ALB	albumin	3.96	0.0006	-1.52	0.5300	-6.02	0.0000
APOA1	apolipoprotein A1	3.21	0.0167	-	-	-3.80	0.0065
APOH	apolipoprotein H	4.72	0.0506	-	-	-3.09	0.2070
C3	complement C3	2.81	0.0371	-	-	-3.53	0.0206
C9	complement C9	5.01	0.0058	-	-	-4.24	0.0198
CFB	complement factor B	6.07	0.3350	-	-	-4.79	0.4270
CP	ceruloplasmin	1.97	0.0123	1.33	0.4830	-1.48	0.2210
CRABP1	cellular retinoic acid binding protein 1	1.26	0.0038	-	-	-1.47	0.0001
F2	coagulation factor II, thrombin	1.44	0.3540	-	-	-1.50	0.2650
FGA	fibrinogen alpha chain	5.51	0.0687	-	-	-4.15	0.2050
FGB	fibrinogen beta chain	4.16	0.0206	-	-	-3.39	0.0726
FGG	fibrinogen gamma chain	3.72	0.0112	-	-	-3.33	0.0207
FN1	fibronectin 1	2.23	0.0340	-	-	-1.74	0.1150
FTL	ferritin light chain	2.54	0.1080	-	-	-	-
HNRNPK	heterogeneous nuclear ribonucleoprotein K	-	-	1.25	0.0617	-	-
HPX	hemopexin	3.17	0.0041	-	-	-2.65	0.0163
KRAS	KRAS proto-oncogene, GTPase	-	-	1.35	0.5660	-	-
MAP2K1	mitogen-activated protein kinase kinase 1	-	-	1.64	0.2100	-	-
MAP2K2	mitogen-activated protein kinase kinase 2	-	-	1.62	0.2270	1.65	0.1660
MAP3K5	mitogen-activated protein kinase kinase kinase 5	2.12	0.0167	-	-	-1.28	0.3750
MAPK14	mitogen-activated protein kinase 14	1.30	0.2020	-	-	-	-
NR3C1	nuclear receptor subfamily 3 group C member 1	2.13	0.3830	-	-	-	-
PLG	plasminogen	3.21	0.0168	-	-	-3.57	0.0271
RALB	RAS like proto-oncogene B	1.38	0.1200	-	-	-	-
RAP1B	RAP1B, member of RAS oncogene family	-	-	1.34	0.4890	-	-
RBP1	retinol binding protein 1	1.77	0.3600	-	-	-2.06	0.1860
RBP3	retinol binding protein 3	-	-	1.30	0.5260	1.52	0.1570
RRAS	RAS related	1.73	0.0294	-	-	-1.47	0.1520
SERPINA1	serpin family A member 1	6.89	0.0885	1.93	0.6770	-7.87	0.0015
SERPINA3	serpin family A member 3	10.50	0.0081	-	-	-7.14	0.0004
SERPIND1	serpin family D member 1	2.15	0.0910	-	-	-2.38	0.0832
SOD2	superoxide dismutase 2	-	-	1.20	0.4130	1.22	0.3890
STAT3	signal transducer and activator of transcription 3	1.92	0.3190	1.57	0.4270	-	-
TF	transferrin	4.79	0.0007	-	-	-4.18	0.0019
TRADD	TNFRSF1A associated via death domain	-1.38	0.4860	-1.50	0.3290	-	-
TTR	transthyretin	4.73	0.0031	-	-	-4.37	0.0052

Figure 9. Parental RHC suppresses postischemic acute phase response in F1 retinae. The acute phase response pathway represents systemic proinflammatory responses triggered by tissue injury that modify immune function, metabolism, oxidative stress, etc. Displayed is the IPA version of this pathway for Comparison 3 (see Supplementary Fig. S4 for Comparisons 1 and 2 for this same canonical), with differentially expressed proteins colored *red* (upregulated) or *green* (downregulated), based on FC. The heat map shows the directional FC, by comparison,

Investigative Ophthalmology & Visual Science

for each protein in the canonical, ranked by expression FC for C1. Note that many of the same proteins that are upregulated in mice from untreated parents (*shades of red*, Comparison 1) are downregulated in mice from RHC-treated parents (*shades of green*, Comparison 3), reflecting the robust inhibition of this component of ischemic injury as a result of F0 RHC treatment. Note the intra-and intercellular distributions (nucleus vs. cytoplasm vs. plasma) of the proteins in this systemic canonical. A tabulated version of this canonical is provided with the fold changes and *P* values for each protein in the canonical and each respective comparison.

ischemic phenotype of untreated controls (C3), all of which yielded a cornucopia of insights into the mechanisms by which intergenerational neuroprotection is established. As a result of space limitations applicable to any journal, herein we offered mechanistic details on the basic components of a mere three of these signaling networks; however, our results are publicly available for further analyses of other pathways and proteins of potential scientific and/or clinical interest.

From both a mechanistic and therapeutic standpoint, some of our most perceptive findings are related to the ischemia-protective effects of parental RHC on visual transduction cycle proteins. Given that the entire process of vision begins in rod photoreceptors and that, in the rod-dominant mouse eye, 97% of all photoreceptors are rods,[35] the ischemia-induced changes we found in the rod proteome are indicative of impairments in both the activation and the recovery phases of the visual transduction cycle and are likely responsible for part or all of the 30% ± 4% reduction in the a-wave amplitude of the rod-generated electroretinogram a-wave that we recorded in untreated mice. Specifically, mounting an activation (hyperpolarization) response to incoming photons would be impaired with less rhodopsin available to absorb them and less cGMP hydrolyzed per a given photonic load as a result of the lower overall catalytic power driving the closure (and resultant hyperpolarization) of cGMP-gated ion channels (secondary to ischemia-induced reductions in the levels and functionality of the co-amplifiers transducin and PDE6). The recovery phase would also be impaired as a result of lower GTPase activity, secondary to ischemia-induced reductions in R9AP. In turn, the 63% improvement in photoreceptor-specific a-wave amplitude (and 83% improvement in the more distal, photoreceptor-dependent b-wave amplitude) that we measured in F1-*RHC mice likely resulted from a remodeled rod cell proteome in which ischemia-induced losses in opsin and transducin-α are completely abrogated and levels of the alpha subunit of the cGMP-gated cation channel and S-arrestin, critical to establishing the dark current and the recovery phase of the transduction cycle, respectively, are increased. Specifically, the normalization of opsin and transducin-α (GNAT1) expression levels, the increased hydrolysis of cGMP secondary to increases in levels of phosphodiesterase, and the enhancement of the time of visual excitation resulting from increases in phosducin expression are all consistent with a more stabilized activation phase of the transduction cycle. In turn, ischemia-induced impairments in the recovery phase of the transduction cycle would be countered by enhanced rhodopsin inactivation secondary to higher levels of rhodopsin kinase by the normalization of GTPase activity and the hydrolysis of bound GTP secondary to the greater deactivation of G-protein signaling (caused by elevations in RGS9 and S-arrestin) and by augmented expression levels of the key proteins responsible for the depolarized phenotype (dark current), most notably the catalyst guanylate cyclase. Overall, this rod proteome profile likely accounts for the significantly smaller loss of the a-wave amplitude (11% ± 2%) in the scotopic ERGs that we recorded in the postischemic retinae of F1-*RHC mice.

Dramatic changes in the levels of key signaling proteins responsible for the regulation and signaling functions of the actin cytoskeleton were another RHC-mediated protective mechanism we identified and probed in detail. The complex cytoskeletal network formed by actin is integral to key dynamic processes such as cell motility, intracellular transport, and axon guidance, as well as endocytosis and exocytosis; moreover, many signal transduction systems use the actin cytoskeleton as a subcellular localization scaffold. Playing central roles in regulating these processes are members of the Rho family of small GTPases, including RhoA and Rac (Ras superfamily members), CDC42, and Rho-associated protein kinase (ROCK), which, after activation by various classes of transmembrane receptors (i.e., integrin receptors, receptor tyrosine kinases, and G protein-coupled receptors), integrate and transmit signals to downstream effector proteins involved in orchestrating cytoskeletal dynamics. Although they are not as well studied or appreciated as being critical to cell function (and cell injury) as many other better known biochemical networks, our findings point to parental RHC exerting ubiquitous, functionally, and structurally protective effects on a number of proteins integral to homeostatic cytoskeletal dynamics,[36] including those affecting cell shape and motility, intra- and intercellular protein and vesicular transport and signaling,[37] organelle biogenesis and movement,[38] dendritic plasticity and axon guidance, the formation of filopodia and lamellipodia, and endocytosis/exocytosis.

We also provided proteomic and bioinformatic detail regarding the acute-phase response proteins[39] involved in the multi-pronged homeostatic defense against systemic-level inflammatory and immune aspects of retinal ischemic injury. Indeed, the APR was the top canonical for both C1 and C3. Our results revealed night-and-day differences in the expression of major APR proteins in the ischemic retinae of F1-*RHC mice born to RHC-treated parents relative to retinae of F1-CTL mice descendant from untreated control parents. Although single-cell proteomics will ultimately provide even more elegant insights into how a given therapeutic affords protection against pathology at the level of specific retinal neurons, Müller cells, and even the retinal and choroidal vasculature, one distinct advantage to preclinical, in situ sampling of whole tissues is the resultant capture of intravascular proteins that can contribute to a broader, integrated understanding of the many ways injury and injury resilience are ultimately manifested at the tissue level, as we did here. Of note, the coagulant system was also a top-ranked canonical for both C1 and C3 (although the overall changes in protein expression were "anti-" to one another), and the complement system also placed in the top five canonicals for C3, underscoring the previous point about systemic-level injury/protection mechanisms.

There are several limitations of our study, many of which warrant further study. One is that we investigated the inher-

Investigative Ophthalmology & Visual Science

itance of an induced, neuroprotective phenotype in F1 offspring resulting from exposing both parents to the epigenetic stimulus prior to mating, which leaves it unclear at present whether only paternal or maternal treatment would also result in the manifestation of ischemic resilience, and to the same extent. We also did not assess whether the retinae in mice from F2 or subsequent generations exhibited ischemic resilience. Regarding the aforementioned fundamental features of intergenerational inheritance, we investigated the retinal phenotype in the progeny of the mice that received the therapeutic treatment. Measures of the underlying epigenetic changes involving DNA methylation, post-translational histone modifications, and noncoding RNAs in both germ cells and in the tissue of impact (i.e., the retina) that are collectively responsible for mediating these changes in phenotype are still needed. Moreover, our proteomic analysis did not include the phosphoproteome[40] or other post-translationally modified protein families known to be critically involved in signaling roles; these data will eventually be essential to gaining a more complete picture of how the resilient proteome is established. Although we used outbred mice of both sexes for our functional outcome studies, we only used male mice for our proteomic analyses; sex-dependent differences may exist with respect to the mechanisms by which injury resilience is achieved. And, as alluded to above in regard to the APR, the retinal proteomes we report here should be considered a "net" response of a set of heterogeneous changes in protein expression occurring in distinct retinal neuronal subsets, Müller and other cells in the glial lineage, endothelial and smooth muscle cells, and even changes occurring in the blood. Finally, the time dependency of the results of our analyses and their implications should also be underscored. Retinae were harvested 10 days after ischemia, shortly after our electrophysiologic assessments of functional outcome at 7 days postischemia, so the proteome profiles reported here do not necessarily represent the acute phase of a dynamic postischemic response nor ones representative of long-term recovery, but somewhere intermediate between the two. To this point, few of the changes in the retinal protein profile we measured in response to ischemia, with and without parental RHC, were found at the RNA level in response to ischemia, with and without postconditioning, in rats[41]; the same is true for respective pathway analyses in this and our study. However, beyond species differences, this is not necessarily unexpected given that we measured retinae at 10 days postischemia and Roth's group measured at 1 day postischemia, and that mRNA abundance does not necessarily translate to protein abundance.[42,43]

One additional translational note: Determining what minimum magnitude, duration, and frequency of systemic hypoxia are required to induce the heritable, adaptive phenotype we report here is of keen interest to us, but our RHC stimulus is not sacrosanct. Other intermittent systemic hypoxia treatments,[18] remote limb conditioning,[44,45] or a pharmacological mimic[46] of either that ultimately modulates the expression of these proteins in a similar manner may someday serve as a viable therapeutic for reducing the incidence of ischemic retinopathy.

In conclusion, the biologic complexities characterizing intergenerational inheritance, particularly in mammals, are broad and deep. Here, we "started at the end" by identifying the injury-resilient proteome of the functionally protected F1 retina and dissecting in detail a few specific signaling networks that are modified as a result of this differential expression profile. Elegant and nontrivial causal studies will be needed to parse the relative contributions of distinct proteins and pathways and confirm their participation in establishing tissue protection. But, for now, we hope our fundamentally novel finding that heritability can be modified to promote an innate injury or disease resilience in offspring will provide a compelling precedent for exploring other manifestations of inducible, beneficial phenotypes being transmitted across generations.

Acknowledgments

Supported by grants from the National Eye Institute, National Institutes of Health (EY018607 to JMG; NIH P30 GM106392 to JJG); by a Sigma Xi Grant-in-Aid-of Research (JCH); and by the Louisiana Lions Eye Foundation. We also thank Nicholas Lanson, Jr., Krystal Belmonte, and Moriah Harman for expert technical assistance with this study.

JMG conceived the study; JCH and JJG designed the proteomics experiments; JCH and JJG performed the proteomics; JCH, JJG, and JMG analyzed data and interpreted experimental results; JCH prepared figures; and JCH, JJG, and JMG drafted, edited, and revised the manuscript and approved the final version of the manuscript.

Disclosure: **J.C. Harman,** None; **J.J. Guidry,** None; **J.M. Gidday,** None

References

1. Allis CD, Jenuwein T. The molecular hallmarks of epigenetic control. *Nat Rev Genet*. 2016;17:487–500.
2. Hunter RG, McEwen BS. Stress and anxiety across the lifespan: structural plasticity and epigenetic regulation. *Epigenomics*. 2013;5:177–194.
3. Jiang S, Postovit L, Cattaneo A, Binder EB, Aitchison KJ. Epigenetic modifications in stress response genes associated with childhood trauma. *Front Psychiatry*. 2019;10:808.
4. Kanherkar RR, Bhatia-Dey N, Csoka AB. Epigenetics across the human lifespan. *Front Cell Dev Biol*. 2014;2:49.
5. Sen P, Shah PP, Nativio R, Berger SL. Epigenetic mechanisms of longevity and aging. *Cell*. 2016;166:822–839.
6. Wang Y, Liu H, Sun Z. Lamarck rises from his grave: parental environment-induced epigenetic inheritance in model organisms and humans. *Biol Rev Camb Philos Soc*. 2017;92:2084–2111.
7. Perez MF, Lehner B. Intergenerational and transgenerational epigenetic inheritance in animals. *Nat Cell Biol*. 2019;21:143–151.
8. Skvortsova K, Iovino N, Bogdanovic O. Functions and mechanisms of epigenetic inheritance in animals. *Nat Rev Mol Cell Biol*. 2018;19:774–790.
9. Boskovic A, Rando OJ. Transgenerational epigenetic inheritance. *Annu Rev Genet*. 2018;52:21–41.
10. van Steenwyk G, Roszkowski M, Manuella F, Franklin TB, Mansuy IM. Transgenerational inheritance of behavioral and metabolic effects of paternal exposure to traumatic stress in early postnatal life: evidence in the 4th generation. *Environ Epigenet*. 2018;4:dvy023.
11. Cunningham AM, Walker DM, Nestler EJ. Paternal transgenerational epigenetic mechanisms mediating stress phenotypes of offspring. *Eur J Neurosci*. 2019; https://doi.org/10.1111/ejn.14582.
12. Feinberg AP, Fallin MD. Epigenetics at the crossroads of genes and the environment. *JAMA*. 2015;314:1129–1130.

13. Bowers ME, Yehuda R. Intergenerational transmission of stress in humans. *Neuropsychopharmacology*. 2016;41:232–244.
14. Hausenloy DJ, Barrabes JA, Botker HE, et al. Ischaemic conditioning and targeting reperfusion injury: a 30 year voyage of discovery. *Basic Res Cardiol*. 2016;111:70.
15. Li S, Hafeez A, Noorulla F, et al. Preconditioning in neuroprotection: from hypoxia to ischemia. *Prog Neurobiol*. 2017;157:79–91.
16. Zhu Y, Zhang Y, Ojwang BA, Brantley MA, Jr, Gidday JM. Long-term tolerance to retinal ischemia by repetitive hypoxic preconditioning: role of HIF-1alpha and heme oxygenase-1. *Invest Ophthalmol Vis Sci*. 2007;48:1735–1743.
17. Stowe AM, Altay T, Freie AB, Gidday JM. Repetitive hypoxia extends endogenous neurovascular protection for stroke. *Ann Neurol*. 2011;69:975–985.
18. Gonzalez-Rothi EJ, Lee KZ, Dale EA, Reier PJ, Mitchell GS, Fuller DD. Intermittent hypoxia and neurorehabilitation. *J Appl Physiol*. 2015;119:1455–1465.
19. Leak RK, Calabrese EJ, Kozumbo WJ, et al. Enhancing and extending biological performance and resilience. *Dose Response*. 2018;16:1559325818784501.
20. Mattson MP, Moehl K, Ghena N, Schmaedick M, Cheng A. Intermittent metabolic switching, neuroplasticity and brain health. *Nat Rev Neurosci*. 2018;19:63–80.
21. Dattilo M, Newman NJ, Biousse V. Acute retinal arterial ischemia. *Ann Eye Sci*. 2018;3:1–13.
22. Fortmann SD, Grant MB. Molecular mechanisms of retinal ischemia. *Curr Opin Physiol*. 2019;7:41–48.
23. Antonetti DA, Klein R, Gardner TW. Diabetic retinopathy. *N Engl J Med*. 2012;366:1227–1239.
24. Duh EJ, Sun JK, Stitt AW. Diabetic retinopathy: current understanding, mechanisms, and treatment strategies. *JCI Insight*. 2017;2:e93751.
25. Zhou D, Ding J, Ya J, et al. Remote ischemic conditioning: a promising therapeutic intervention for multi-organ protection. *Aging*. 2018;10:1825–1855.
26. Belmonte KC, Harman JC, Lanson NA, Gidday JM. Intra- and inter-generational changes in the cortical DNA methylome in response to therapeutic intermittent hypoxia in mice. *Physiol Genomics*. 2020;52:20–34.
27. Yang F, Shen Y, Camp DG, 2nd, Smith RD. High-pH reversed-phase chromatography with fraction concatenation for 2D proteomic analysis. *Expert Rev Proteomics*. 2012;9:129–134.
28. Pascale CL, Martinez AN, Carr C, et al. Treatment with dimethyl fumarate reduces the formation and rupture of intracranial aneurysms: role of Nrf2 activation. *J Cereb Blood Flow Metab*. 2020;40:1077–1089.
29. Vizcaino JA, Csordas A, del-Toro N, et al. 2016 update of the PRIDE database and its related tools. *Nucleic Acids Res*. 2016;44:D447–D456.
30. Peterson AC, Russell JD, Bailey DJ, Westphall MS, Coon JJ. Parallel reaction monitoring for high resolution and high mass accuracy quantitative, targeted proteomics. *Mol Cell Proteomics*. 2012;11:1475–1488.
31. MacLean B, Tomazela DM, Shulman N, et al. Skyline: an open source document editor for creating and analyzing targeted proteomics experiments. *Bioinformatics*. 2010;26:966–968
32. Gapp K, Soldado-Magraner S, Alvarez-Sanchez M, et al. Early life stress in fathers improves behavioural flexibility in their offspring. *Nat Commun*. 2014;5:5466.
33. Arai JA, Li S, Hartley DM, Feig LA. Transgenerational rescue of a genetic defect in long-term potentiation and memory formation by juvenile enrichment. *J Neurosci*. 2009;29:1496–1502.
34. Benito E, Kerimoglu C, Ramachandran B, et al. RNA-dependent intergenerational inheritance of enhanced synaptic plasticity after environmental enrichment. *Cell Rep*. 2018;23:546–554.
35. Jeon CJ, Strettoi E, Masland RH. The major cell populations of the mouse retina. *J Neurosci*. 1998;18:8936–8946.
36. Merino F, Pospich S, Raunser S. Towards a structural understanding of the remodeling of the actin cytoskeleton. *Semin Cell Dev Biol*. 2020;102:51–64.
37. Moujaber O, Stochaj U. The cytoskeleton as regulator of cell signaling pathways. *Trends Biochem Sci*. 2019;45:96–107.
38. Cardanho-Ramos C, Faria-Pereira A, Morais VA. Orchestrating mitochondria in neurons: cytoskeleton as the conductor. *Cytoskeleton*. 2020;77:65–75.
39. Ahmed MS, Jadhav AB, Hassan A, Meng QH. Acute phase reactants as novel predictors of cardiovascular disease. *ISRN Inflamm*. 2012;2012:953461.
40. Harman JC, Guidry JJ, Gidday JM. Comprehensive characterization of the adult ND4 Swiss Webster mouse retina: using discovery-based mass spectrometry to decipher the total proteome and phosphoproteome. *Mol Vis*. 2018;24:875–889.
41. Kadzielawa K, Mathew B, Stelman CR, Lei AZ, Torres L, Roth S. Gene expression in retinal ischemic post-conditioning. *Graefes Arch Clin Exp Ophthalmol*. 2018;256:935–949.
42. Edfors F, Danielsson F, Hallstrom BM, et al. Gene-specific correlation of RNA and protein levels in human cells and tissues. *Mol Syst Biol*. 2016;12:883.
43. Liu Y, Beyer A, Aebersold R. On the dependency of cellular protein levels on mRNA abundance. *Cell*. 2016;165:535–550.
44. Brandli A, Johnstone DM, Stone J. Remote ischemic preconditioning protects retinal photoreceptors: evidence from a rat model of light-induced photoreceptor degeneration. *Invest Ophthalmol Vis Sci*. 2016;57:5302–5313.
45. Heyman SN, Leibowitz D, Mor-Yosef Levi I, et al. Adaptive response to hypoxia and remote ischaemia preconditioning: a new hypoxia-inducible factors era in clinical medicine. *Acta Physiol*. 2016;216:395–406.
46. Dhillon S. Roxadustat: first global approval. *Drugs*. 2019;79:563–572.

Investigative Ophthalmology & Visual Science